The Company of
Biologists

RESEARCH ARTICLE

Ceramide synthase homolog Tlc4 maintains nuclear envelope integrity via its Golgi translocation

Yasuhiro Hirano[1,*], Yusuke Ohno[2], Yoshino Kubota[1], Tatsuo Fukagawa[1], Akio Kihara[2], Tokuko Haraguchi[1] and Yasushi Hiraoka[1,*]

ABSTRACT

Maintaining the integrity of the nuclear envelope (NE) is essential for preventing genomic DNA damage. Recent studies have shown that enzymes that catalyze lipid synthesis are involved in NE maintenance, but the underlying mechanism remains unclear. Here, we found that the ceramide synthase (CerS) homolog in the fission yeast *Schizosaccharomyces pombe* Tlc4 (SPAC17A2.02c) suppressed NE defects in cells lacking the NE proteins Lem2 and Bqt4. Tlc4 possesses a TRAM/LAG1/CLN8 domain that is conserved in CerS proteins and functions through its non-catalytic activity. Tlc4 was localized at the NE and endoplasmic reticulum, similar to CerS proteins, and also showed unique additional localization at the cis- and medial-Golgi cisternae. Growth and mutation analyses revealed that Golgi localization of Tlc4 was tightly linked to its activity of suppressing the defects in the double-deletion mutant of Lem2 and Bqt4. Our results suggest that Lem2 and Bqt4 control the translocation of Tlc4 from the NE to the Golgi, which is necessary for maintaining NE integrity.

KEY WORDS: Nuclear envelope, Ceramide, Golgi, Lem2, Bqt4, Tlc4

INTRODUCTION

The eukaryotic genome is organized within the nucleus and surrounded by the nuclear envelope (NE). The NE consists of inner and outer nuclear membranes, and is continuous with the ER membrane. The integrity of the NE is crucial for retaining the nuclear permeability barrier, thereby maintaining cell viability (Webster and Lusk, 2016). However, the NE is dynamic and undergoes repeated disassembly and reassembly during the mitotic cell cycle in higher eukaryotic cells (open mitosis) (Güttinger et al., 2009; Lajoie and Ullman, 2017; Ungricht and Kutay, 2017). Thus, cells have mechanisms to seal nuclear membrane holes during NE reformation to maintain NE integrity.

To seal membrane holes during NE reformation at the end of mitosis, the endosomal sorting complex required for transport-III (ESCRT-III) is transiently recruited to the reforming NE by charged multivesicular body protein 7 (CHMP7 in metazoans, Chm7 in the budding yeast *Saccharomyces cerevisiae*, and Cmp7 in the fission yeast *Schizosaccharomyces pombe* and *Schizosaccharomyces*

[1]Graduate School of Frontier Biosciences, Osaka University, Suita 565-0871, Japan. [2]Faculty of Pharmaceutical Sciences, Hokkaido University, Sapporo 060-0812, Japan.

*Authors for correspondence (yhira@fbs.osaka-u.ac.jp; hiraoka@fbs.osaka-u.ac.jp)

Y. Hirano, 0000-0001-7339-4053; T.F., 0000-0001-8564-6852; A.K., 0000-0001-5889-0788; T.H., 0000-0002-3813-6785; Y. Hiraoka, 0000-0001-9407-8228

japonicus) (Gu et al., 2017; Olmos et al., 2015; Pieper et al., 2020; Vietri et al., 2015; Von Appen et al., 2020). Recent studies have demonstrated that Lem2, a member of the conserved Lap2β–emerin–Man1 (LEM)-domain NE protein family, functions as a nuclear adaptor for CHMP7 (Gu et al., 2017; Von Appen et al., 2020; Webster et al., 2016). Vps4, an AAA family ATPase, is loaded on the NE reforming sites and induces the disassembly of ESCRT-III to complete NE sealing (Gu et al., 2017; Vietri et al., 2015; Williams and Urbé, 2007). Such nuclear membrane sealing mechanisms are highly conserved across diverse eukaryotes, including organisms with 'closed mitosis', such as *S. pombe* (Dey et al., 2020; Gu et al., 2017). ESCRT-III is involved in sealing membrane rupture during mitosis and interphase in mammalian cells, illustrating its general role in maintaining NE integrity (Denais et al., 2016; Raab et al., 2016).

The inner nuclear membrane protein Lem2 appears to play a broad role in maintaining NE integrity. In *S. pombe,* Lem2, which shares a LEM-like domain (HEH/LEM domain) with metazoan Lem2, is involved in many cellular processes, such as heterochromatin formation (Banday et al., 2016; Barrales et al., 2016; Tange et al., 2016), exosome-mediated RNA elimination (Martín Caballero et al., 2022), nuclear size regulation and NE–endoplasmic reticulum (ER) boundary formation with the ER protein Lnp1 (homolog of human Lunapark) (Hirano et al., 2020; Kume et al., 2019), and nuclear membrane maintenance with ESCRT-III components (Gu et al., 2017; Lee et al., 2020; Pieper et al., 2020; Thaller et al., 2021; Von Appen et al., 2020) and the inner nuclear membrane protein Bqt4 (Hirano et al., 2018; Kinuagsa et al., 2019; Tange et al., 2016). Bqt4 was initially identified as a protein that tethers telomeres to the NE (Chikashige et al., 2009), and its role in nuclear membrane maintenance has been inferred because the double deletion of *lem2[+]* and *bqt4[+]* confers a synthetic lethal phenotype accompanied by nuclear membrane rupture (Kinuagsa et al., 2019; Tange et al., 2016).

We attempted to understand how Lem2 and Bqt4 maintain NE integrity in *S. pombe*. In a previous study, we performed multicopy suppressor screening of the synthetic lethality of the *lem2Δbqt4Δ* double-deletion mutant and identified only one suppressor, *elo2[+]* (Kinuagsa et al., 2019). Elo2 is a fatty acid (FA) elongase that generates very long-chain FAs (VLCFAs; >C20). VLCFAs are less abundant than long-chain FAs (C11–C20), accounting for only a small percentage of the total FAs in cells. However, they play crucial roles that cannot be substituted by long-chain FAs: most saturated and mono-unsaturated VLCFAs are incorporated into ceramides. Ceramides are the hydrophobic backbone of sphingolipids, one of the major lipid components of eukaryotic membranes, and are composed of a FA and a long-chain base. VLCFA-containing ceramides/sphingolipids play important roles in skin barrier formation and neural functions in mammals (Mizutani et al., 2009; Imgrund et al., 2009; Kihara, 2016). The most abundant

1

ceramide species in *S. pombe* is C24 phytoceramide, which contains phytosphingosine as a long-chain base moiety and C24:0 VLCFA as a FA moiety (Garton et al., 2003; Kinugsa et al., 2019).

To identify additional suppressors of synthetic lethality of *lem2Δbqt4Δ*, in this study, we used a moderate condition for suppressor screening using the *lem2*-shut-off strain expressing a hypomorphic mutant of *bqt4*. In this screening, we found a new suppressor *tlc4*[+] (SPAC17A2.02c), which shares a TRAM/LAG1/CLN8 (TLC)-domain with the ceramide synthase (CerS) family.

RESULTS

Identification of multicopy suppressors of the synthetic lethal phenotype of *lem2* and *bqt4*

To identify suppressors of the synthetic lethal phenotype of *lem2Δbqt4Δ*, we expressed a Bqt4 hypomorphic mutation in a *lem2*-shut-off *bqt4Δ* background (*nmt81p-FLAG-lem2-IAA-HA lem2Δ bqt4Δ*), which was used as a screening host. As a Bqt4 hypomorphic mutant, we tested Bqt4-R48E and Bqt4-K106E/R107E mutants because the protein binding activity in APSES (named for Asm1p, Phd1p, Sok2p, Efg1p and StuAp) domains has been reported to decrease via different mutations: R48E (approximately 6.0-fold reduction in the protein binding activity of Bqt4 to Lem2) (Hu et al., 2019a) and K83E/K106E/R107E (approximately 2.6-fold reduction in the protein binding activity of Bqt4 to Rap1) (Hu et al., 2019b). We confirmed that R48E and K106E/R107E mutations weakened Bqt4 functions: these *bqt4* mutants showed growth defects that were less severe than those of *bqt4Δ* upon *lem2* shut-off via thiamine addition (Fig. 1, compare 'vec' in each background).

Using this strategy, we screened approximately 30,000 colonies in total (approximately 3000 and 27,000 colonies for R48E and K106E/R107E, respectively) and identified eight suppressors excluding *lem2*[+] and *bqt4*[+]: *elo2*[+], *lnp1*[+], *apq12*[+], *SPAC17A2.02c*[+], *erg2*[+], *ice2*[+], *cnx1*[+] and *ubc4*[+] (Fig. 1). These showed different extents of suppression: *elo2*[+], *SPAC17A2.02c*[+], *erg2*[+], and *cnx1*[+] rescued the synthetic lethality of *lem2Δbqt4Δ*, and *lnp1*[+], *apq12*[+], *ice2*[+] and *ubc4*[+] rescued the growth defect in *lem2Δ*-bearing *bqt4* hypomorphic mutants. *elo2*[+], *lnp1*[+] and *apq12*[+] have been identified as genes that show genetic interactions with *lem2* and/or *bqt4* (Hirano et al., 2020; Kinuagsa et al., 2019; Tange et al., 2016); *erg2*[+], *SPAC17A2.02c*[+], *cnx1*[+], *ice2*[+] and *ubc4*[+] were identified as suppressors in this study. Erg2, known as C-8 sterol isomerase, is involved in ergosterol biosynthesis (Hull et al., 2012). As the C-8 sterol isomerase

activity-deficient mutant of Erg2 lost its growth recovery activity (Fig. S1A,B), it is likely that ergosterol biosynthesis is required for NE integrity. Cnx1, also known as calnexin, recognizes a specific sugar group, Glc1Man5-9GlcNAc2, and is involved in the quality control of glycoproteins (Parlati et al., 1995). Deletion of either *lem2* or *bqt4* exacerbated the growth defect of the temperature-sensitive mutant of *cnx1* (*cnx1Δ23-437*) (Fig. S1C), indicating genetic interactions among *cnx1*, *lem2* and *bqt4*. Overexpression of the C-terminal Cnx1 fragment, which is required for survival from nitrogen-starvation-induced cell death (Elagoz et al., 1999; Núñez et al., 2015), rescued the growth defect (Fig. S1D), suggesting that Cnx1 functions as an anti-apoptotic factor in the context of the synthetic lethal process of *lem2* and *bqt4* double deletion. In PomBase (https://www.pombase.org/) (Harris et al., 2022), SPAC17A2.02c is predicted as a seven-time transmembrane protein containing a TRAM/LAG1/CLN8 (TLC) homology domain, which is conserved in CerS family proteins, such as Lac1 and Lag1, suggesting that SPAC17A2.02c is implicated in ceramide synthesis. As the increased level of ceramides rescued the synthetic lethality of *lem2Δbqt4Δ* (Kinuagsa et al., 2019), we hypothesized that the overexpression of *SPAC17A2.02c*[+] might also affect the ceramide levels in *lem2Δbqt4Δ* cells. Therefore, we focused on the mechanism by which *SPAC17A2.02c*[+] rescued the synthetic lethality of *lem2Δbqt4Δ*.

SPAC17A2.02c is a conserved protein distinct from CerS proteins

We searched for homologs of SPAC17A2.02c using BLAST and analyzed the phylogenetic relationships among them. SPAC17A2.02c was categorized into a clade composed of TLCD proteins (blue-shaded clade; Fig. 2A), which was isolated from a clade containing CerS proteins (red-shaded clade; Fig. 2A) (Mallela et al., 2016; Winter and Ponting, 2002). TLCD proteins are highly conserved from yeast to humans, with six homologs (TLCD1, 2, 3A, 3B, 4 and 5) in humans and two homologs (YPR114W and TDA4) in the budding yeast *S. cerevisiae* (Mallela et al., 2016). SPAC17A2.02c was the sole TLCD protein in *S. pombe* and showed the highest homology with proteins in the TLCD4 clade (green clade; Fig. 2A). Therefore, we named this gene *tlc4*[+].

To examine the functional conservation of *S. pombe* Tlc4, two *S. cerevisiae* homologs, YPR114W and TDA4, were expressed in the *lem2*-shut-off *bqt4Δ* strain, and its cell growth was observed in the presence or absence of thiamine (Fig. 2B). In these
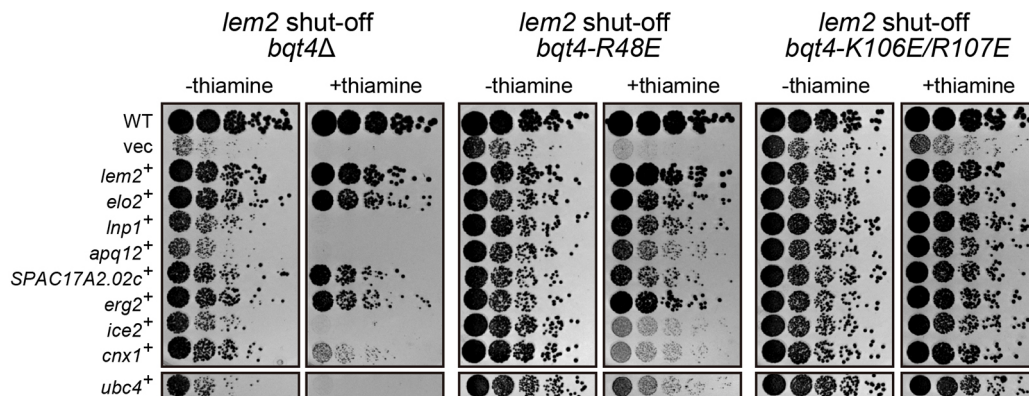
Fig. 1. Multicopy suppressors rescue the growth defect in the *lem2Δbqt4Δ* double-deletion mutant. Genes indicated on the left were expressed using the multicopy plasmid in *lem2*-shut-off *bqt4Δ* (shut-off), *lem2*-shut-off *bqt4Δ bqt4p-bqt4-R48E* (R48E), and *lem2*-shut-off *bqt4Δ bqt4p-bqt4-K106E/R107E* (K106E/R107E) cells. Five-fold serially diluted cells were spotted on EMMG plates with or without thiamine, and the growth of these cells was observed after four days. Images are representative of at least three independent experiments.
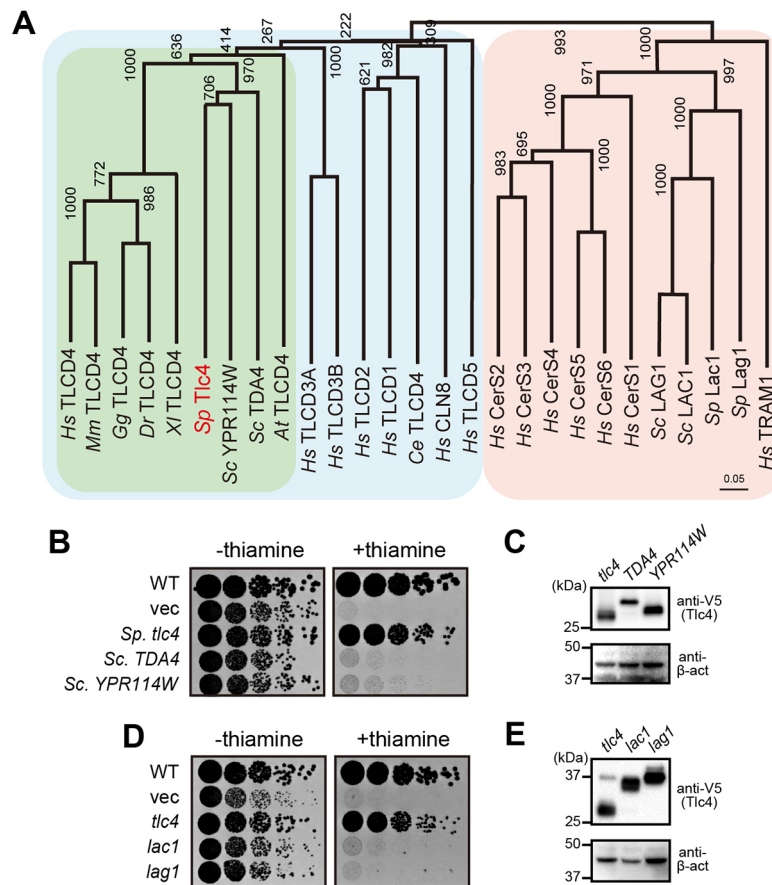
Fig. 2. Tlc4 belongs to the TLCD family and forms a different clade from the CerS family. (A) Phylogenic analysis of Tlc4 (SPAC17A2.02c) and CerS homologs. Tlc4 and CerS homologs were searched using BLAST using *Schizosaccharomyces pombe* Tlc4 and Lac1 as queries, respectively. A phylogenic tree was generated from the amino acid sequences of the TLC domain (TLCD) using ClustalX2. Numbers at the branch points represent the bootstrap probabilities. Red-, blue- and green-colored clades represent the CerS family, TLCD family and Tlc4 protein homologs, respectively. Abbreviations of species are as follows: *Hs*, *Homo sapiens*; *Mm*, *Mus musculus*; *Gg*, *Gallus gallus*; *Xl*, *Xenopus laevis*; *Dr*, *Danio rerio*; *At*, *Arabidopsis thaliana*; *Ce*, *Caenorhabditis elegans*; *Sp*, *Schizosaccharomyces pombe*; *Sc*, *Saccharomyces cerevisiae.* Species, nomenclatures and accession numbers used are as follows: *Hs* CerS1 (NM_001290265.1, NP_001277194.1); *Hs* CerS2 (NM_022075.5, NP_071358.1); *Hs* CerS3 (NM_001290341.2, NP_001277270.1); *Hs* CerS4 (NM_024552. 3, NP_078828.2); *Hs* CerS5 (NM_147190.5, NP_671723); *Hs* CerS6 (NM_001256126.2, NP_001243055.1); *Sp* Tlc4 (NM_001019659.2, NP_594236.1); *Sp* Lag1 (NM_001356001.1, NP_001342862.1); *Sp* Lac1 (NM_001022018.2, NP_596102.1); *Sc* Lag1 (NM_001179083.1, NP_011860.1); *Sc* Lac1 (NM_ 001179574.3, NP_012917.3); *Sc* TDA4 (NM_001181774.1, NP_012650.1); *Sc* YPR114W (NM_001184211.1, NP_015439.1); *Hs* TLCD1 (NM_138463.4, NP_612472.1); *Hs* TLCD2 (NM_001164407.2, NP_001157879.1); *Hs* TLCD3A (NM_024792.3, NP_079068.1); *Hs* TLCD3B (NM_031478.6, NP_113666.2); *Hs* TLCD4 (NM_152487.3, NP_689700.1); *Hs* TLCD5 (NM_001198670.2, NP_001185599.1); *Mm* TLCD4 (NM_001355678.2, NP_001342607.2); *Gg* TLCD4 (NM_001277557.4, NP_001264486.2); *Xl* TLCD4 (NM_001092735.1); *Dr* TLCD4 (NM_001005924.2, NP_001005924.1); *Ce* TLCD4 (NM_058435.8, NP_ 490836.1); *At* TLCD4 (NM_179214.2, NP_849545.1); *Hs* CLN8 (NM_018941.4, NP_061764.2); *Hs* TRAM1 (NM_014294.6, NP_055109.1). (B) Cell growth with increased expression of *S. cerevisiae* TLCD genes. *S. cerevisiae* TLCD genes (*TDA4* and *YPR114W*) were cloned under the *adh1* promoter and introduced into *lem2*-shut-off *bqt4*Δ cells. The cells were spotted on the EMMG plates with or without thiamine in five-fold serial dilutions together with positive (*tlc4*) and negative (*vec*) controls and incubated at 30°C for 4 days. (C) Protein expression levels. Tlc4, TDA4 and YPR114W were expressed as V5-tagged proteins under the *adh1* promoter in *S. pombe* cells, and the protein expression levels were determined by western blotting. β-actin was used as a loading control. Antibodies used and molecular weight markers are shown on the right and left, respectively. (D) Cell growth with increased expression of *S. pombe* CerS genes. *S. pombe* CerS genes (*lac1* and *lag1*) were cloned under the *adh1* promoter and introduced into *lem2*-shut-off *bqt4*Δ cells. Cell growth was observed as described in B. (E) Protein expression levels. Tlc4, Lac1 and Lag1 were expressed as V5-tagged proteins, and the protein expression levels were determined by western blotting as described in C. Images are representative of at least two independent experiments.

experiments, the homologs were expressed under the *adh1* promoter, one of the strongest constitutive promoters in *S. pombe*, because a high expression level of Tlc4 was required for growth restoration (Fig. S1E,F). Neither YPR114W nor TDA4 recovered cell growth, although their protein expression levels were almost identical to those of Tlc4 (Fig. 2B,C), suggesting that *S. pombe* Tlc4 is not close to the TLCD homologs in its functionality. In addition, overexpression of the *S. pombe* CerS proteins Lag1 and Lac1 did not rescue the growth defect upon shut-off (Fig. 2D,E), suggesting that Tlc4 has a function distinct from that of CerS proteins.

Overexpression of Tlc4 suppresses the pleiotropic phenotypes of *lem2Δbqt4Δ*

As Tlc4 rescued the synthetic lethality of *lem2Δbqt4Δ*, we examined the effects of Tlc4 overexpression on nuclear protein leakage and ceramide levels, which are striking defects in *lem2Δbqt4Δ* cells (Kinuagsa et al., 2019; Tange et al., 2016). For this purpose, Tlc4 was overexpressed in *lem2*-shut-off *bqt4*Δ cells expressing GFP–GST–NLS as a nuclear protein marker. Nuclear protein leakage was determined as the ratio of fluorescence intensity of GFP–GST–NLS in the nucleus to that in the cytoplasm (N/C) (Fig. 3A,B). In the
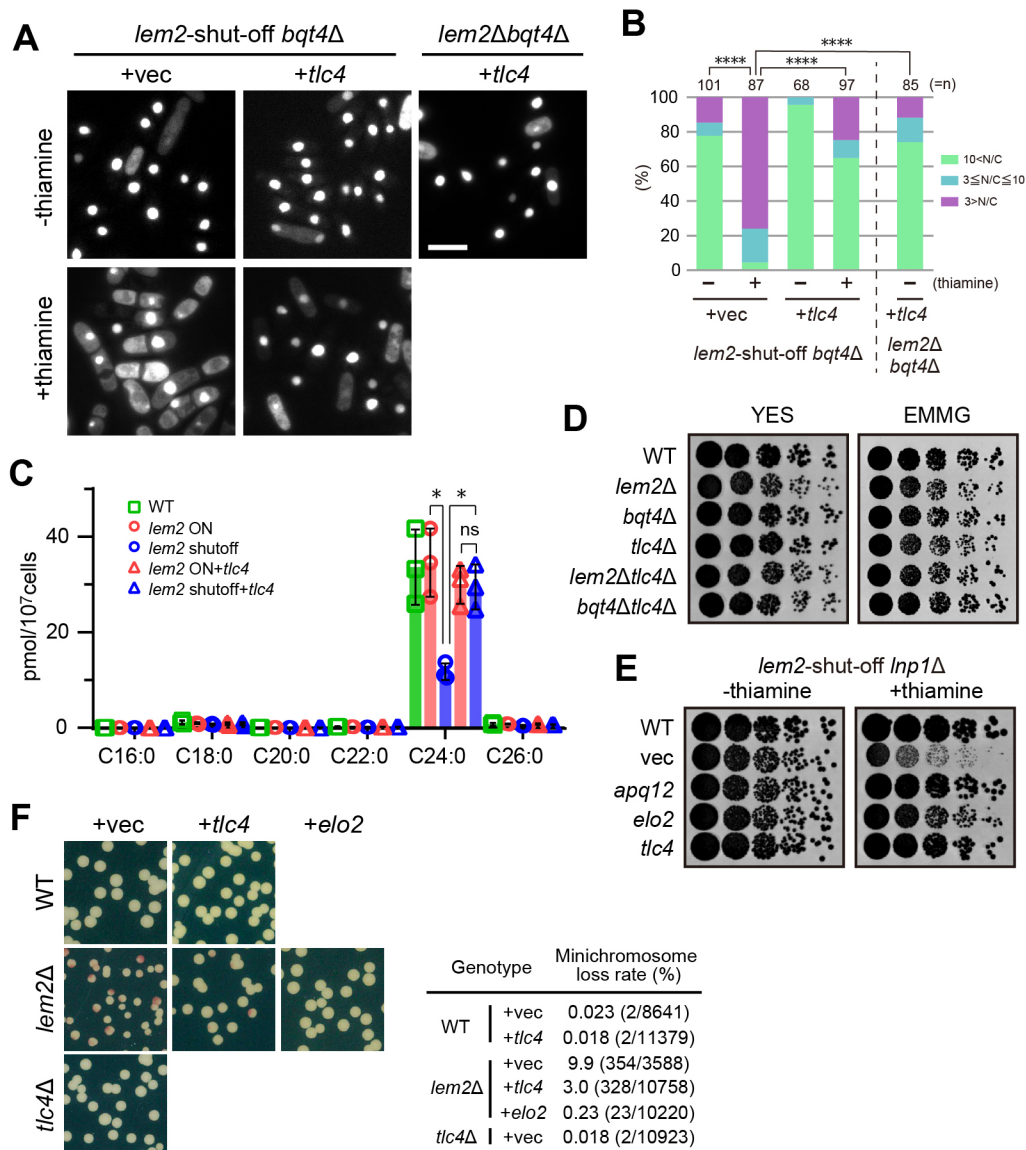
Fig. 3. Tlc4 suppresses the pleiotropic defects in *lem2Δbqt4Δ* cells. (A) Suppression of nuclear protein leakage. GFP–GST– NLS was expressed in *lem2*-shut-off *bqt4Δ* or *lem2Δbqt4Δ* cells together with *tlc4* (+*tlc4*) and a control vector (+vec). The cells were cultured in EMMG in the presence or absence of thiamine. The GFP–GST–NLS signal was observed. Scale bar: 10 μm. (B) Quantification of the nuclear protein leaking phenotype. Fold enrichment of the GFP–GST–NLS signal in the nucleus (nucleus/cytoplasm, N/C) observed in A was quantified and classified into three levels according to its leakage: non-leaking (N/C≥10), moderate (10>N/C≥ 3) and severe N/C<3). Percentages of cells were plotted as a cumulative bar chart. *n* indicates the total cell number counted. ****P<0.001 via χ^2 test. (C) Phytoceramide levels. The *lem2* shut-off *bqt4Δ* (open circles) and *lem2* shut-off *bqt4Δ* strains overexpressing Tlc4 (open triangles) were cultured in EMMG with (blue) or without thiamine (red). After extracting lipids from the cells, phytoceramides composed of C20 phytosphingosine and a non-hydroxy FA were quantified via liquid chromatography coupled with tandem mass spectrometry (LC-MS/MS). The determined phytoceramide species, which have differing FA chain lengths and levels of unsaturation, are indicated at the bottom (e.g. phytoceramide containing saturated C24 FA as C24:0). Levels of phytoceramides were determined from three independent experiments. Bars show the mean±s.d. ns, not significant; *P<0.05 (Dunnett's test versus *lem2* shut-off). (D) Cell growth in the *lem2*, *bqt4* and *tlc4* deletion strains. The cells were spotted on YES and EMMG plates in five-fold serial dilutions and incubated at 30°C for 2 (YES) and 4 (EMMG) days. (E) Cell growth with increased expression levels of *tlc4* in *lem2*-shut-off *lnp1Δ* cells. The cells were spotted on the EMMG plate with or without thiamine in five-fold serial dilutions and incubated at 30°C for 4 days. (F) Minichromosome loss rates in *lem2Δ* cells with or without *tlc4*+ overexpression. *tlc4* or *elo2* were expressed in WT and *lem2Δ* cells harboring the minichromosome. The cells were grown on the YE plate medium. Half-sectored colonies were counted and the minichromosome loss rates are shown. The numbers in brackets represent the number of colonies counted. Images in A are representative of three independent experiments. Images in D,E and F are the results of single experiments.

positive control, nuclear proteins severely leaked upon shut-off, indicating nuclear membrane breakage (+vec, +thiamine; Fig. 3A). This leaky phenotype was significantly suppressed by Tlc4 overexpression (+*tlc4*, +thiamine) (Fig. 3A,B). In addition, the nuclear protein leakage was weakened in the *lem2Δbqt4Δ* background (see *lem2Δbqt4Δ* in Fig. 3A), indicating that Tlc4

suppressed the nuclear membrane breakage. We also determined the levels of phytoceramides, the most abundant ceramide class in yeast, using liquid chromatography coupled with tandem mass spectrometry (LC-MS/MS) in *lem2* shut-off *bqt4Δ* cells overexpressing Tlc4. The levels of the phytoceramide composed of a non-hydroxy saturated C24 fatty acyl chain (C24:0) decreased

upon shut-off and were restored by Tlc4 overexpression (Fig. 3C). These results suggest that Tlc4 plays a role in ceramide synthesis.

Next, we investigated the genetic interactions among *lem2⁺*, *bqt4⁺* and *tlc4⁺*. The double-deletion mutants *lem2Δtlc4Δ* and *bqt4Δtlc4Δ* showed no growth defects under rich or minimal growth conditions (Fig. 3D). To identify the functions of Lem2 and Bqt4 that are restored by Tlc4, we examined whether Tlc4 could rescue the defects of Lem2. For this purpose, we used the *lem2*-shut-off *lnp1Δ* strain. Because *lem2Δ* confers a growth defect with *lnp1Δ* (Hirano et al., 2020), we expected that the overexpression of Tlc4 would rescue the growth defect of *lem2*-shut-off *lnp1Δ* cells if Tlc4 complemented Lem2 functions. The results showed that overexpression of Tlc4 recovered the growth of *lem2*-shut-off *lnp1Δ* cells, along with Apq12, which is a known suppressor of its growth defect (Hirano et al., 2020) (Fig. 3E). To further examine whether Tlc4 rescued *lem2Δ*-specific phenotypes, we performed a minichromosome loss assay (Fig. 3F). Overexpression of Tlc4 decreased the loss rate (from 9.9 to 3.0%); however, the effect was weaker than that of Elo2 (0.23%). Additionally, *tlc4Δ* displayed a low loss rate comparable to that of the wild type (WT versus *tlc4Δ* in Fig. 3F), suggesting that Tlc4 is indirectly involved in chromosome segregation. Collectively, these results suggest that Tlc4 complements the Lem2 function. These results indicate that Tlc4 suppresses the pleiotropic phenotypes of *lem2Δbqt4Δ*.

Tlc4 plays a non-catalytic role in ceramide synthesis

The overexpression of Tlc4 showed quite similar phenotypic suppression effects for *lem2Δbqt4Δ* with Elo2. As Elo2 also functions in ceramide synthesis by elongating the carbon chains of FAs (Kinuagsa et al., 2019), and Tlc4 has a TLC domain conserved in CerS proteins, we investigated the relationship between Tlc4 and Elo2 in ceramide synthesis. Considering the chemical reaction flow of ceramide synthesis, in which VLCFAs are synthesized by FA elongase and then conjugated to a long-chain base by CerS, it is speculated that Tlc4 functions in ceramide synthesis downstream of Elo2. Therefore, we tested whether Tlc4 functions downstream of Elo2 by introducing *tlc4Δ* into *lem2* shut-off *bqt4Δ* cells overexpressing Elo2. If this hypothesis was correct, *tlc4Δ* would have disrupted the growth recovery activity of Elo2. However, *tlc4Δ* did not disrupt the growth recovery activity of Elo2 (Fig. 4A), indicating that Tlc4 functions in ceramide synthesis but not downstream of Elo2.

A possible alternative pathway to restore ceramide synthesis is that Tlc4 functions upstream of Elo2 independently of CerS activity. However, determining whether Tlc4 functions upstream of Elo2 is difficult because the essential gene *elo2⁺* cannot be deleted (Kinugsa et al., 2019). To elucidate whether Tlc4 had any CerS enzymatic activity, we first determined the levels of ceramides in *S. pombe* cells overexpressing or lacking *tlc4⁺*. Neither overexpression nor deletion of *tlc4⁺* altered the overall ceramide levels (Fig. 4B), suggesting that Tlc4 has little to no CerS activity. This result is consistent with the fact that the active site residues of the CerS proteins are not fully conserved in Tlc4 (Fig. S2A). Two sequential histidine residues in the fourth transmembrane domain function as an active center for ceramide synthesis in CerS proteins (red open square in Fig. S2A) (Kageyama-Yahara and Riezman, 2006; Levy and Futerman, 2010; Spassieva et al., 2006; Winter and Ponting, 2002), but Tlc4 had only one histidine residue (H149) at the corresponding site (see arrow in the middle panel in Fig. S2A). To further assess the contribution of H149 residue to the growth recovery activity of Tlc4, we substituted this histidine residue with alanine (H149A), expressed it in the *lem2*-shut-off *bqt4Δ* strain, and
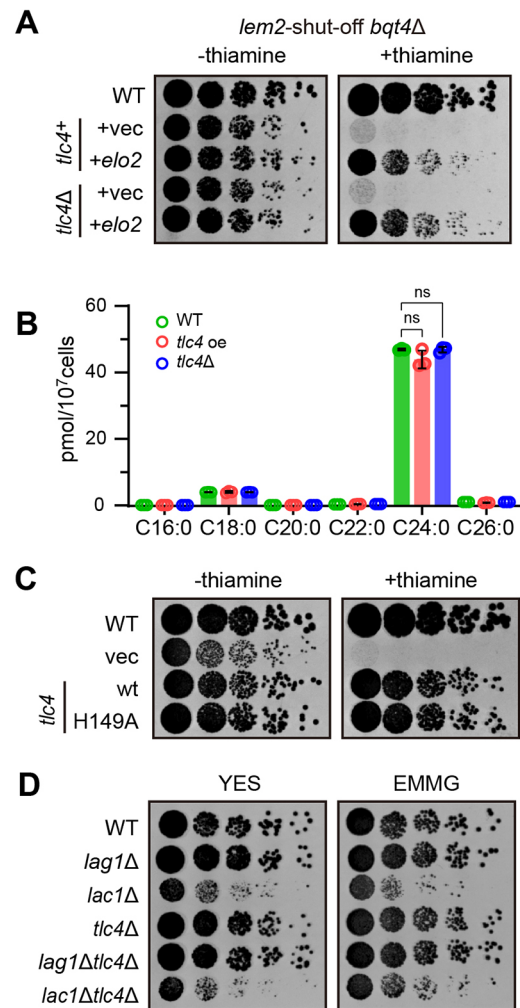
Fig. 4. Tlc4 has a non-catalytic role in ceramide synthesis. (A) Effect of *tlc4Δ* on the growth recovery by *elo2*. Deletion of *tlc4* was introduced into the *lem2* shut-off *bqt4Δ* strains overexpressing Elo2. The cells were spotted on the EMMG plate with or without thiamine in five-fold serial dilutions and incubated at 30°C for 4 days. (B) Phytoceramide levels. Lipids were extracted from the WT, *tlc4⁺*-overexpressing (*tlc4* oe) and *tlc4* mutant (*tlc4Δ*) cells. Levels of phytoceramides were determined as described in Fig. 3C. Bars show the mean±s.d. ns, not significant. (C) Cell growth in *lem2* shut-off *bqt4Δ* cells expressing a Tlc4 mutant. The cells expressing wild-type (wt) or H149A mutant (H149A) were spotted on the EMMG plate with or without thiamine in five-fold serial dilutions and incubated at 30°C for 4 days. (D) Cell growth in the *lag1*, *lac1,* and *tlc4* deletion strains. The cells were spotted on the YES and EMMG plates in five-fold serial dilutions and incubated at 30°C for 2 (YES) and 4 (EMMG) days. Images in A and C are representative of at least three independent experiments. Images in D are the results of a single experiment.

observed cell growth upon *lem2* shut-off (Fig. 4C). The H149A mutant rescued the growth defect, indicating that the histidine residue was not essential for the growth recovery activity of Tlc4. These results suggest that Tlc4 rescues the synthetic growth defect of *lem2Δbqt4Δ* independent of CerS activity.

Next, we examined whether *tlc4⁺* confers any synthetic lethality to known CerS enzymes. In *S. cerevisiae*, ceramide synthesis is crucial for cell viability, and the double deletion of the CerS enzymes *LAG1* and *LAC1* confers a severe growth defect (Guillas et al., 2001; Schorling et al., 2001). Thus, we examined the homologs of *LAG1* and *LAC1*: *lag1⁺* and *lac1⁺*, respectively. Double deletion of *lag1Δ* and *lac1Δ* (*lag1Δlac1Δ*) conferred synthetic lethality (Fig. S2B) as recently reported (Flor-Parra

et al., 2021). Neither *lag1Δtlc4Δ* nor *lac1Δtlc4Δ* exacerbated the growth defect in *lag1Δ* or *lac1Δ* (Fig. 4D), suggesting that *tlc4⁺* does not genetically interact with *lag1⁺* or *lac1⁺*. This was consistent with the data that overexpression of Lag1 and Lac1 did not restore the synthetic lethality of *lem2Δbqt4Δ* (Fig. 2D). Collectively, our results suggest that Tlc4 plays a non-catalytic role in ceramide synthesis to rescue the synthetic lethality of *lem2Δbqt4Δ* in *S. pombe*.

Tlc4 is localized to the NE/ER, Golgi apparatus and endosomes

We examined the subcellular localization of Tlc4 in comparison with CerS proteins. *S. pombe* CerS proteins, such as Lac1 and Lag1, have been reported to be localized in the ER (Flor-Parra et al., 2021). Here, we observed the localization of GFP-tagged Tlc4 (Tlc4–GFP) with mCherry-tagged Lac1 (mCherry–Lac1) or Lag1 (Lag1–mCherry) in *S. pombe* cells (Fig. 5A,B). Tlc4–GFP was localized to the cytoplasmic foci, NE, perinuclear ER and peripheral ER. NE and ER localization of Tlc4 was confirmed via double staining with Ish1–mCherry and ADEL–GFP as the NE and ER marker proteins, respectively (Fig. S3A,B) (Asakawa et al., 2022;

Hirano et al., 2020). The cytoplasmic foci of Tlc4–GFP showed the most prominent differences from those of CerS proteins (mCherry–Lac1 and Lag1–mCherry). To identify the subcellular structures in which the cytoplasmic foci of Tlc4–GFP were localized, Tlc4–GFP was expressed in the cells with various subcellular structural markers: mCherry–Sed5, Mnn9–mCherry and Sec71–mCherry for the cis-, medial- and trans-Golgi, respectively (Ishii et al., 2016; Kurokawa et al., 2014); Vps4–mCherry for endosomes (Pieper et al., 2020); and FM4-64 for vacuoles. The results showed that Tlc4–GFP foci colocalized with the cis- and medial-Golgi, but not with the trans-Golgi (Fig. 5C, arrowheads). In particular, most of the Tlc4 foci (80.6±14.2%; mean±s.d.) were colocalized with the medial-Golgi marker Mnn9–mCherry and vice versa (70.6±13.9%) (Fig. 5C). Furthermore, Tlc4–GFP foci were also localized in late endosomes, marked by Vps4–mCherry, but less frequently (Fig. 5D). Even when localized, the Tlc4–GFP signal was weak (Fig. 5D; arrows). In contrast, the Tlc4–GFP foci did not colocalize with vacuoles (Fig. S3C). The localization of Tlc4–GFP in the cis- and medial-Golgi and late endosomes, distinct from that of CerS proteins, might reflect that Tlc4, but not CerS proteins, rescue the growth defect of *lem2Δbqt4Δ*.
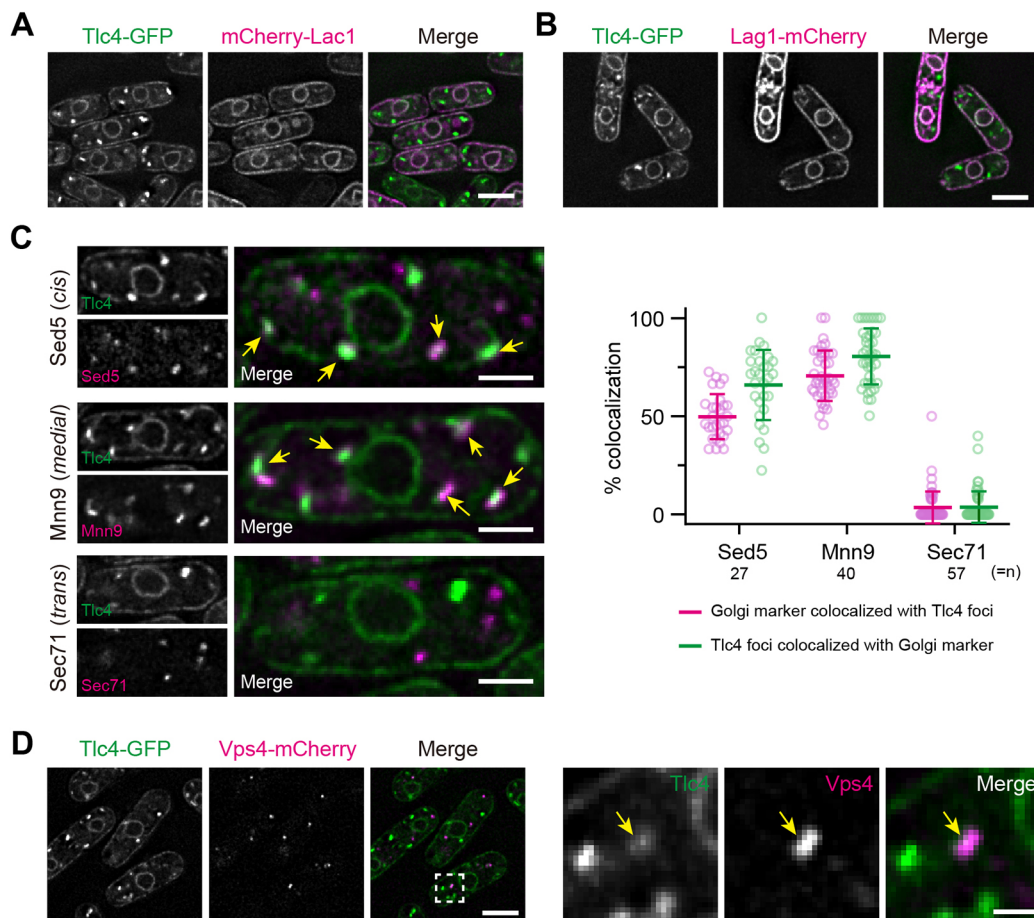
Fig. 5. Tlc4 is localized to the NE/ER, cis- and medial-Golgi, and late endosomes. Representative images of Tlc4 localization. GFP-tagged Tlc4 (Tlc4–GFP) was co-expressed with subcellular structural markers and visualized using fluorescence microscopy. (A,B) Tlc4–GFP was co-expressed with mCherry-tagged Lac1 (mCherry–Lac1) (A) or Lag1 (Lag1–mCherry) (B). Scale bars: 5 μm. (C) Tlc4–GFP was co-expressed with mCherry-tagged cis- (Sed5, top), medial- (Mnn9, middle) and trans- (Sec71, bottom) Golgi markers. Arrows indicate the Tlc4 foci that were colocalized with Golgi markers. Scale bars: 5 μm. Quantification of the percentage of colocalization is shown on the right panel. The percentage of Golgi markers colocalized with Tlc4 foci was calculated for each cell (magenta), and the percentage of Tlc4 foci colocalized with Golgi markers was quantified for each cell (green). Values were plotted as mean±s.d. *n* denotes the cell number counted for quantification. (D) Tlc4–GFP was co-expressed with the late endosome marker, Vps4–mCherry. The dashed square region in the left panel is enlarged on the right side. Arrows indicate the Tlc4 foci that were colocalized with the late endosomes. Scale bars: 5 μm (left); 1 μm (right). Images are representative of at least three independent experiments.

Lem2 and Bqt4 are required for the Golgi localization of Tlc4

To investigate whether Lem2 and Bqt4 affect Tlc4 localization in the Golgi, Tlc4–GFP and Mnn9–mCherry (a marker for the medial-Golgi) were expressed in *lem2*-shut-off *bqt4Δ* cells, and their signals were observed upon *lem2* shut-off by thiamine addition. The number of Tlc4 foci was significantly decreased by the shut-off condition, but the number of Mnn9–mCherry foci was unchanged (Fig. 6A); for their quantification, compare '–thi' and '+thi' of the '*lem2* shut-off *bqt4Δ*' plots in Fig. 6B. The protein levels of Tlc4 and Mnn9 were almost unchanged before and after the shut-off compared with the levels of β-actin as the control (Fig. 6C). These results suggest that both Lem2 and Bqt4 are required for the Golgi localization of Tlc4. A single deletion of *lem2Δ* or *bqt4Δ* did not alter the Golgi localization of the Tlc4 foci (Fig. S3D), further supporting this idea. To investigate whether the translocation of Tlc4 from the NE to Golgi is inhibited in the *lem2* shut-off condition, we quantified the percentage of fluorescence intensity of Tlc4–GFP localized at the Golgi and NE in the presence or absence of thiamine (Fig. 6D). The Tlc4–GFP signal at the Golgi substantially decreased upon *lem2* shut-off (from 7.3% to 2.3%; compare '–thi' and '+thi' at the Golgi in Fig. 6D), whereas that at the NE increased (from 8.5% to 11.0%, Fig. 6D). Thus, it is likely that translocation of Tlc4 from the NE to the Golgi is inhibited in the absence of Lem2 and Bqt4, leading to the accumulation of Tlc4 at the NE.

Subsequently, we tested the effect of Tlc4 overexpression on its localization in *lem2*-shut-off *bqt4Δ* cells. We overexpressed Tlc4 in *lem2*-shut-off *bqt4Δ* cells expressing Tlc4–GFP and Mnn9–mCherry (*tlc4* op; see Table S1 for detail) and counted the number of Tlc4 foci in *lem2* shut-off by thiamine addition. The result showed that localization of Tlc4–GFP at the Golgi was restored by Tlc4 overexpression in *lem2*-shut-off *bqt4Δ* cells (Fig. 6E) (for their quantification, compare '–thi' and '+thi' of the '*tlc4* op' plots in Fig. 6B). Moreover, the Tlc4–GFP signal at the Golgi increased by Tlc4 overexpression (from 2.3% to 12.1%; compare the '+thi Golgi' plots of '*lem2* shut-off *bqt4Δ*' with those of '*tlc4* op' in Fig. 6D). Although the Golgi signal decreased upon thiamine addition even in the Tlc4-overexpressing cells (from 14.5% to 12.1%), it was still significantly higher than that in *lem2*-shut-off *bqt4Δ* cells in the absence of thiamine (7.3%; leftmost column in Fig. 6D). These results indicate that the Golgi localization of Tlc4 decreases in the absence of Lem2 and Bqt4, and is restored by Tlc4 overexpression.

Golgi localization of Tlc4 is linked to its growth recovery activity

Because Lem2 and Bqt4 are required for the Golgi localization of Tlc4, we further analyzed the relationship between Golgi localization and the growth recovery activity of Tlc4. For this purpose, we attempted to obtain Tlc4 mutants that lost their growth recovery activity. We inspected the amino acid sequence alignment of Tlc4 and CerS proteins and focused on H149 and R214 in Tlc4, as H149 corresponds to the active center in Lac1 and R214 is one of the most conserved amino acid residues, except for H149 (see Fig. S2A, red arrows).

H149 and R214 of Tlc4 were substituted with alanine (Tlc4-H149A and Tlc4-R214A, respectively) and expressed in *lem2*-shut-off *bqt4Δ* cells. Cells expressing the Tlc4-H149A mutation (H149A; Fig. 4B, Fig. 7A) showed no apparent growth defects in a spot assay compared to the WT cells as the control (WT; Fig. 7A), whereas cells expressing the Tlc4-R214A mutation showed decreased growth activity under shut-off conditions (R214A; Fig. 7A). The *lem2*-shut-off *bqt4Δ* cells expressing the double

mutation of H149A and R214A of Tlc4 (Tlc4-H149A/R214A) showed severe growth defects under shut-off conditions (H149A/R214A; Fig. 7A). We confirmed that the expression levels of these mutant proteins were similar (Fig. 7B), and protein degradation of these mutants was not observed under any conditions tested (Fig. S4A,B). Additionally, AlphaFold2 (Mirdita et al., 2022) predicted that their structural differences were relatively low (Fig. S4C). Thus, it is unlikely that the loss of function of R214A mutants is caused by the misfolding of the protein. Therefore, the R214 residue of Tlc4 is likely critical for the growth activity of *S. pombe*.

Next, the *S. pombe* strain harboring a Tlc4 mutation at the R214 residue was used to evaluate the relationship between Golgi localization and the growth recovery activity of Tlc4. The subcellular localization of Tlc4 mutants was observed via fluorescence microscopy (Fig. 7C–E). The localization of mCherry–Sed5, Mnn9–mCherry and Sec71–mCherry was also observed in the same cells as markers of the cis-, medial- and trans-Golgi, respectively. Images showed that Tlc4-R214A–GFP and Tlc4-H149A/R214A–GFP were localized in the NE but not in the Golgi (Fig. 7D,E). In contrast, Tlc4-H149A–GFP was localized in both the NE and Golgi, similarly to Tlc4–GFP (Fig. 7C), suggesting that the R214 residue of Tlc4 is important for Golgi localization. The results of the growth and localization assays of the mutants indicate that the Golgi localization of Tlc4 is related to its growth recovery activity.

The Golgi localization property of TLCD proteins is conserved in human cells

Finally, we investigated the evolutionary conservation of *S. pombe* Tlc4 and human TLCD proteins. Assessment of their functional conservation in terms of suppression of synthetic lethality in *lem2Δbqt4Δ* cells was difficult because of the low expression level in *S. pombe* (Fig. S6). To evaluate the intercellular localization of human (h) TLCD protein homologs (hTLCD1, 2, 3A, 3B, 4 and 5), they were expressed as EGFP-tagged proteins and co-stained with Golgi or ER markers in hTERT-RPE1 cells. Fluorescence images revealed that all hTLCD homologs were localized to the Golgi apparatus (Fig. 8A). Signals of hTLCD1, 3A and 4 were predominantly localized in the Golgi; those of hTLCD2, 3B and 5 were localized in the ER, in addition to the Golgi (Fig. 8A; Fig. S4). To determine whether this Golgi localization of hTLCD4 was conserved in different species, we observed the subcellular localization of hTLCD4–EGFP expressed in *S. pombe* (Fig. 8B). The results showed that hTLCD4–EGFP was mainly localized to the Golgi apparatus in addition to the NE/ER, similarly to that of *S. pombe* Tlc4. These results suggest that the Golgi localization is a conserved property of TLCD homologs, which might share some conserved functions.

DISCUSSION

In this study, we identified Tlc4 and Erg2 as suppressors of the synthetic lethal phenotype of the *lem2Δbqt4Δ* double-deletion mutant. Tlc4 and Erg2 are potential enzymes involved in lipid synthesis.

Tlc4 supports ceramide synthesis upon overexpression despite its lack of CerS activity (Fig. 4). Considering that the VLCFA elonagase Elo2 also rescues the synthetic lethality of cells lacking Lem2 and Bqt4 by increasing the amounts of VLCFAs and ceramides (Kinuagsa et al., 2019), the increase in ceramide species (Fig. 3C) appears to rescue these synthetic lethal phenotypes. However, overexpression of the CerS proteins Lac1 and Lag1 did not rescue the growth defect of *lem2Δbqt4Δ* cells in this study
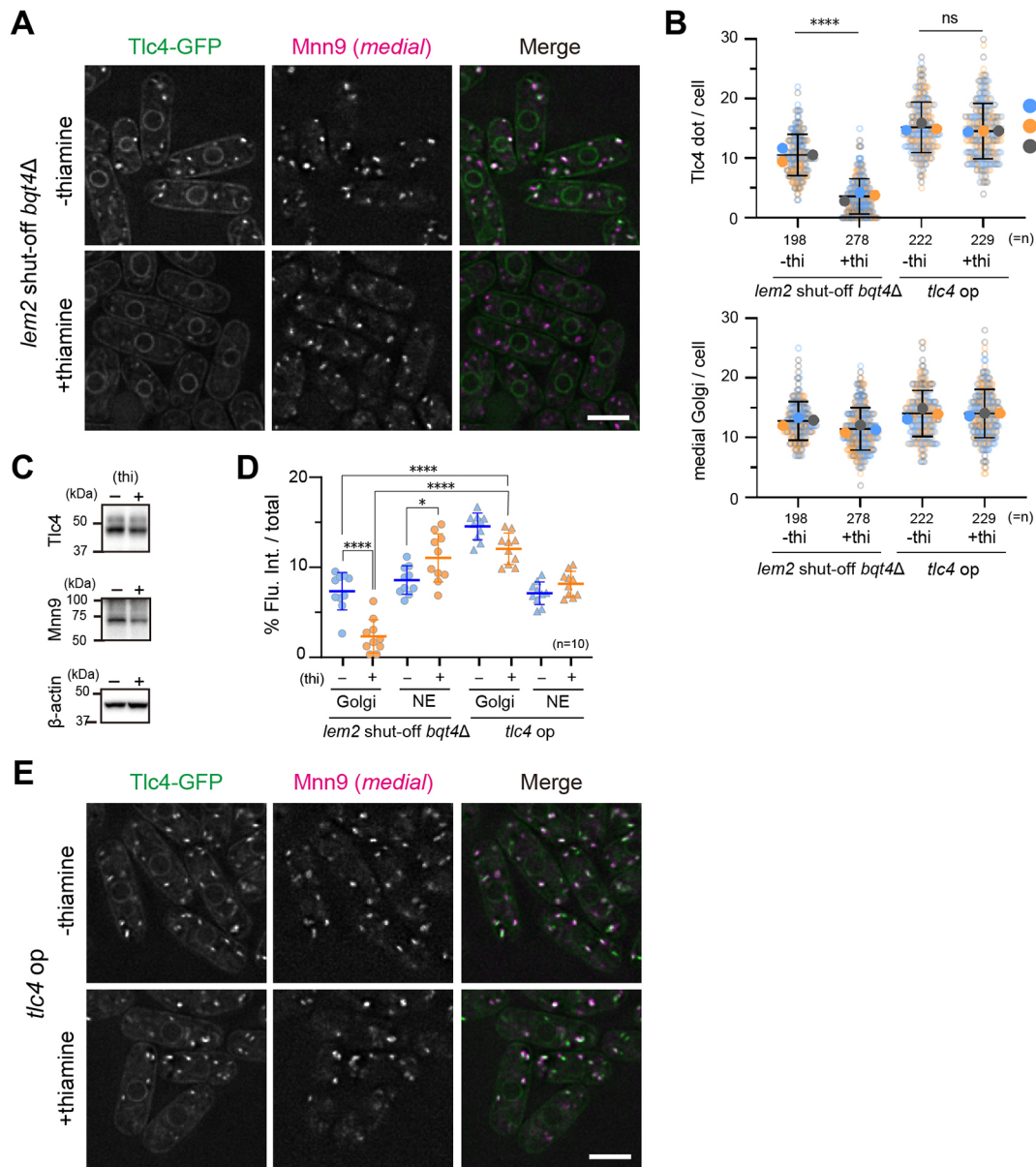
Fig. 6. Lem2 and Bqt4 are required for the Golgi localization of Tlc4. (A) Representative images of Tlc4 localization in *lem2* shut-off *bqt4Δ* cells. The cells were cultured in EMMG in the presence (+thiamine) or absence (–thiamine) of thiamine and visualized with Mnn9–mCherry. Scale bar: 5 μm. (B) Quantification of Tlc4 foci and Golgi numbers. The numbers of Tlc4 foci (top) and Golgi (bottom) in *lem2* shut-off *bqt4Δ* (*lem2* shut-off *bqt4Δ*) or *lem2* shut-off *bqt4Δ* cells overexpressing Tlc4 (*tlc4* op) cells were counted from three independent experiments (shown in blue, orange and gray). Open and closed circles represent the individual measurements and mean of the measurements in each experiment, respectively. Black horizontal lines represent the mean value for all data shown with s.d. *n* at the bottom represents the total number of cells counted. ns, not significant; ****$P<0.0001$ (unpaired two-tailed Student's *t*-test). (C) Protein levels of Tlc4. The *lem2* shut-off *bqt4Δ* cells expressing Tlc4–GFP and Mnn9–mCherry were cultured in the presence or absence of thiamine for 12 h. Protein levels of Tlc4 and Mnn9 were determined by western blotting with the anti-GFP and anti-mRFP antibodies, respectively. β-actin was used as the loading control. The protein molecular size marker is shown on the left. (D) Quantification of fluorescence intensity at the Golgi and NE. The *lem2* shut-off *bqt4Δ* cells expressing Tlc4–GFP with (*tlc4* op) or without (*lem2* shut-off *bqt4Δ*) *tlc4* overexpression were cultured in EMMG in the presence (+thi, orange) or absence (–thi, blue) of thiamine. The fluorescence intensity of Tlc4–GFP in the Golgi, NE and whole cell was quantified from ten cells, the percentage of the fluorescence intensity in the Golgi and NE was calculated, and then the values were plotted. Bold horizontal lines represent the mean value for all data shown with s.d. *$P<0.05$; ****$P<0.0001$ (unpaired two-tailed Student's *t*-test). (E) Representative images of Tlc4 localization in *lem2* shut-off *bqt4Δ* cells overexpressing Tlc4 (*tlc4* op). The cells were cultured and visualized as described in A. Scale bar: 5 μm. Images are representative of at least three independent experiments.

(Fig. 2D), suggesting that another factor(s) is necessary for NE maintenance. Thus, we hypothesize that an alteration in the mechanical properties of the nuclear membrane, such as membrane rigidity resulting from an increase in longer FAs rather than ceramide synthesis, might be important to prevent membrane rupture. This hypothesis is supported by the fact that Erg2 can suppress this phenotype. Erg2 is an enzyme involved in ergosterol biogenesis (Hull et al., 2012). The C-8 sterol isomerase activity of Erg2 is essential for its growth recovery activity (Fig. S1A,B), suggesting that increased ergosterol levels are required to prevent the rupture of the nuclear membrane. As both phenomena, increasing levels of longer FAs and ergosterol, are known to
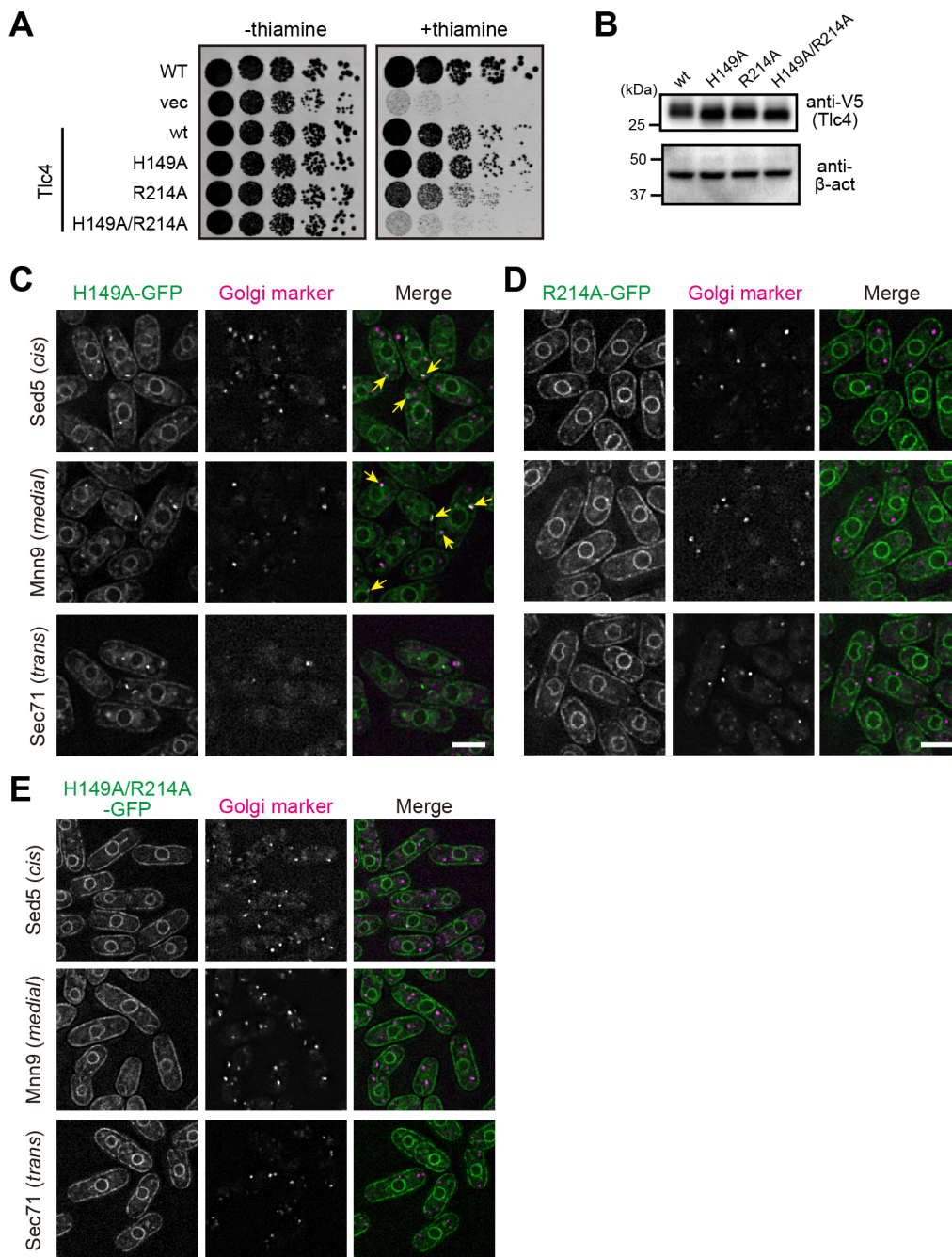
Fig. 7. Translocation of Tlc4 from the ER to Golgi is linked to its growth recovery activity. (A) Cell growth in Tlc4 mutants. Tlc4 wild-type (wt) and point mutants indicated on the left (H149A, R214A and H149A/R214A) were expressed in the *lem2*-shut-off *bqt4Δ* cells. The cells were spotted on the EMMG plate with or without thiamine in five-fold serial dilutions and incubated at 30°C for 4 days. (B) Protein expression levels. Wild-type (wt) Tlc4 and its point mutants indicated on the top were expressed as V5-tagged proteins, and the expression levels of these proteins were determined by western blotting as described in Fig. 2C. (C–E) Representative images of the localization of Tlc4 mutants. H149A (C), R214A (D) and H149A/R214A (E) mutants were co-expressed with Golgi markers indicated on the left. Arrows represent the colocalization of the mutant with the Golgi marker. Scale bars: 5 µm. Images are representative of at least three independent experiments.

increase membrane rigidity, it is likely that the nuclear membrane becomes more fluid and frequently ruptures in the absence of Lem2 and Bqt4. Overexpression of Tlc4 Elo2, or Erg2 might reverse this effect by increasing the membrane rigidity. Accumulating evidence indicates that *de novo* lipid synthesis is involved in the maintenance of NE integrity (Bahmanyar and Schlieker, 2020; Hwang et al., 2019; Kinuagsa et al., 2019; Lee et al., 2020; Penfield et al., 2020). These findings shed light on the importance of the dynamic regulation of the physiological properties of the nuclear membrane.

Although the mechanism by which overexpressed Tlc4 restores ceramide levels remains unknown, we speculate that Tlc4 could be involved in transporting ceramides or VLCFAs from the NE/ER to other organellar components, particularly the cis- and medial-Golgi. The most striking difference between CerS proteins (Lac1 and

Lag1) and Tlc4 was their localization: Lac1 and Lag1 were localized in the ER, whereas Tlc4 was localized in the NE/ER, cis- and medial-Golgi, and endosomes (Fig. 5). Our analyses revealed that the growth recovery activity of Tlc4 and its Golgi localization were closely correlated (Figs 6 and 7). In particular, mutation analysis uncovered a crucial amino acid residue, R214, for the Golgi localization of Tlc4. Although this residue has not been identified as an active site residue of CerS so far, an experiment using Lac1 suggested that the R214 residue of Tlc4 forms an active center in ceramide synthesis from the analogy of the TLC domain conformation. A mutation introduced in the corresponding residue of Lac1 (R291A) did not restore the growth defect of *lac1Δ* cells (Fig. S7), suggesting that the R291A mutation weakened its CerS activity. Consistent with our findings, a previous study reported that
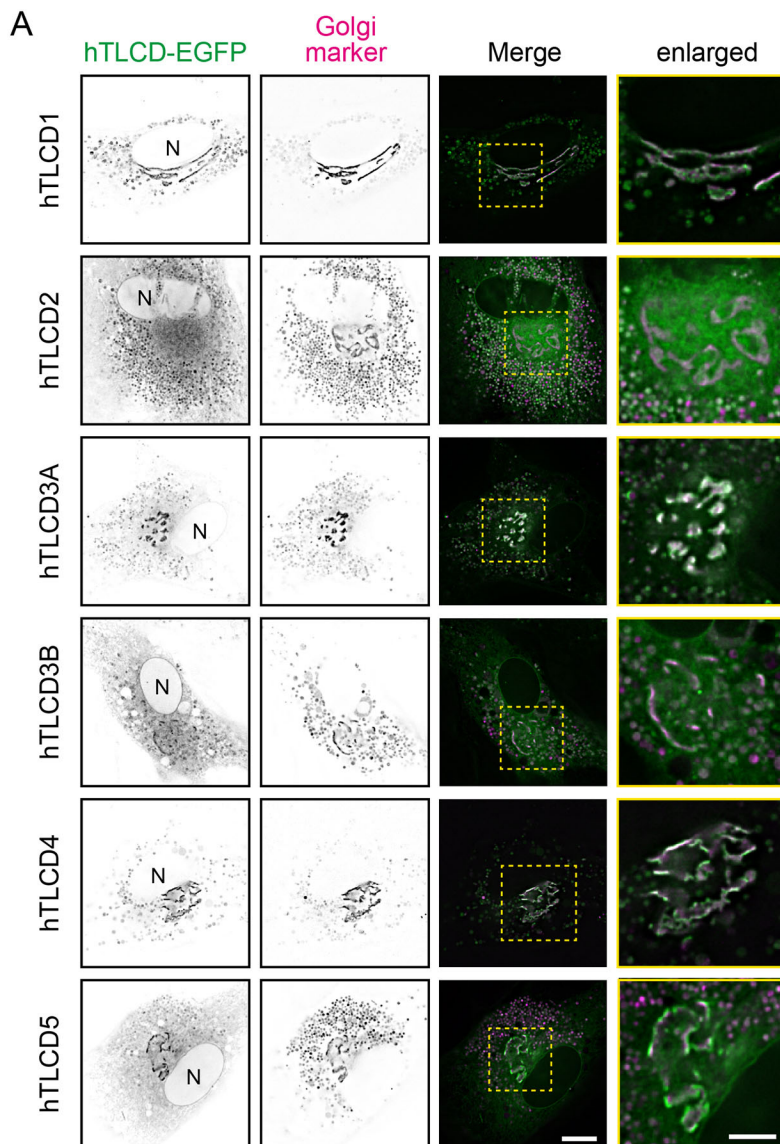
Fig. 8. Human TLCD proteins localize at the Golgi.
(A) Representative images of the localization of human TLCD proteins. GFP-tagged human TLCD homologs (first column; green) and mCherry-tagged Golgi markers (second column; magenta) were transiently expressed in hTERT-RPE1 cells. Merged images are shown in the third column. Yellow square regions are enlarged in the last column. N indicates the position of the nucleus. Scale bars: 10 µm (merge) and 5 µm (enlarged). (B) Representative images of the localization of hTLCD4 in *S. pombe*. hTLCD4–EGFP was expressed with the Golgi marker Mnn9–mCherry. Arrows represent the colocalization of hTLCD4 with the Golgi marker. Scale bar: 5 µm. Images are representative of at least two independent experiments.
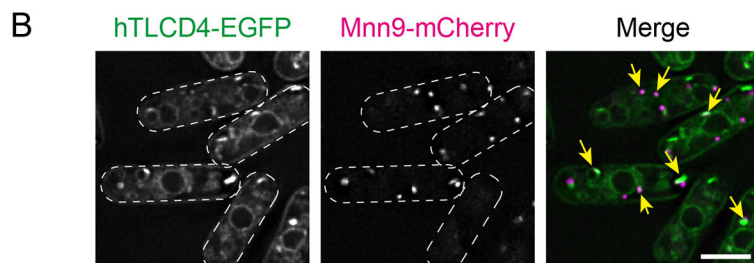
the CerS activity of Lac1 is required for cell growth (Flor-Parra et al., 2021). Thus, our result suggests that R291 in Lac1 forms an active center with the H228 residue. As the double mutation of Tlc4 at the H149 and R214 residues caused a synthetic defect in cell growth, transmembrane regions 4 and 6, where H149 and R214 reside, respectively, might form a binding pocket for ceramide or VLCFAs, which is supported by the three-dimensional conformation of the TLC domain predicted by AlphaFold2 (see Figs S2A and S4). As Lem2 is known to regulate the membrane flow from the NE to other organelles (Kume et al., 2019), Tlc4 might be involved in the ability of Lem2 to transport ceramides or VLCFAs from the NE/ER to Golgi. Ceramides are transported from the ER to the Golgi via non-vesicular transport, supporting our hypothesis. The ceramide transport protein CERT mediates ceramide transport from the ER to the trans-Golgi in mammals (Hanada et al., 2003), and Nvj2 and the tricalbins Tcb1, Tcb2, and Tcb3 mediate the transport in *S. cerevisiae* (Ikeda et al., 2020; Liu et al., 2017; Schlarmann et al., 2021). It has also been reported that Svf1 acts in a parallel pathway to COPII-dependent vesicular transport and Nvj2-mediated non-vesicular transport (Limar et al., 2023). A recent study reported that

hTLCD1/2 interacts with mitochondria and regulates mitochondrial phosphatidylethanolamine composition, although hTLCD1/2 is localized in Golgi and ER (Petkevicius et al., 2022). Considering that TLCD homologs are involved in lipid composition regulation in a different organelle than where the TLCD protein is localized, Tlc4 could potentially transfer ceramides or VLCFAs by connecting the NE and Golgi when it is overexpressed.

In summary, growth and mutation analyses revealed that the Golgi localization of Tlc4 was tightly linked to its activity of suppressing the defects in the double-deletion mutant of Lem2 and Bqt4. Based on these results, we propose a model in which Lem2 and Bqt4 maintain the nuclear membrane by controlling lipid transport from the NE/ER to the Golgi (Fig. S8).

MATERIALS AND METHODS

S. pombe strains, mammalian cell lines and culture media
All *S. pombe* strains used in this study are listed in Table S1. In this study, Edinburgh minimal medium with glutamate (EMMG) or EMMG5S (EMMG with 0.225 mg/ml adenine, leucine, uracil, lysine and histidine) was used as the minimum medium, and yeast extract with supplements (YES) was used as the rich medium (Moreno et al., 1991). Cells were cultured in an appropriate medium at 30°C for 3–5 days, depending on their growth. Strains carrying *lem2Δ* were maintained in EMMG medium to avoid genomic instability, which occurs in rich medium, as previously reported (Hirano et al., 2018, 2020; Kinuagsa et al., 2019; Tange et al., 2016). For selection, 100 µg/ml G418 disulfate (Nacalai Tesque, Kyoto, Japan), 200 µg/ml hygromycin B (FUJIFILM Wako Pure Chemical, Osaka, Japan), 100 µg/ml nourseothricin sulfate (WERNER BioAgents, Jena, Germany) and 100 µg/ml blasticidin S (FUJIFILM Wako Pure Chemical) were added to the medium.

The hTERT-RPE1 cell line was purchased from the American Type Culture Collection (Manassas, VA, USA) (CRL-4000). Cells were cultured in high-glucose Dulbecco's modified Eagle's medium (Nacalai Tesque) supplemented with 10% fetal bovine serum at 37°C in humidified 5% CO_2 atmosphere.

Gene disruption, integration and tagging
Gene disruption, integration, and tagging were performed using a two-step PCR method for direct chromosome integration, as previously described (Bähler et al., 1998; Wach, 1996). Briefly, for the first round of PCR, approximately 500 bp genomic sequences upstream and downstream from the open reading frames (ORFs) of interest were amplified via PCR using KOD One (TOYOBO, Osaka, Japan; KMM-201). These PCR products were used as primers for the second round of PCR to amplify a template sequence containing the selection markers. The resulting PCR product was transformed into *S. pombe* cells for disruption, integration and tagging, and transformants were selected on an appropriate selection plate. The obtained strains were confirmed for correct constructions of disruption, integration and tagging via genomic PCR using KOD Fx neo (TOYOBO; KFX-201) from both the 5′ and 3′ ends. In addition, we performed genomic PCR inside the ORF of the gene of interest to confirm the absence of the ORF in the genome.

Multicopy suppressor screening
The *S. pombe* genomic library pTN-L1 was provided by the National BioResource Project Yeast in Japan. First, we performed a pilot screening: H1N1417 (*h⁻ ura4-D18 leu1-32 lys1⁺::nmt81p-FLAG-lem2-IAA17-HA lem2Δ::kanʳ bqt4Δ::hph aur1ʳ::GFP-Bqt4-R48E*) and H1N1418 (*h⁻ ura4-D18 leu1-32 lys1⁺::nmt81p-FLAG-lem2-IAA17-HA lem2Δ::kanʳ bqt4Δ:: hph aur1ʳ::GFP-Bqt4-K106E/R107E*) cells (1.0×10⁷) were transformed with 0.5 µg of the genomic library, plated on EMMG supplemented with uracil, and incubated at 30°C for 4–5 days. After estimating the transformation efficiency, we screened them using H1N1436 (*h⁻ leu1-32 lys1⁺::nmt81p-FLAG-lem2-IAA17-HA lem2Δ::kanʳ bqt4Δ::hph aur1ʳ:: GFP-Bqt4-K106E/R107E*). First, 3.0×10⁷ cells were transformed with 1.5 µg of the genomic library and incubated at 30°C for 4–5 days on the EMMG plate. In total, approximately 3000 and 27,000 transformants from

Bqt4-R48E and Bqt4-K106E/R107E backgrounds, respectively, were screened. Colonies displaying better growth were picked and re-streaked on the EMMG plate to check the growth recovery, and 192 suppressor colonies (36 and 156 from R48E and K106E/R107E, respectively) were obtained. Plasmids in the cells were isolated using the Cameron method (Cameron et al., 1977). Plasmids containing *lem2⁺* and *bqt4⁺* were screened by PCR analysis (18 and 16 suppressors, respectively). After removing suppressors containing the *elo2⁺*, *lnp1⁺* and *apq12⁺* genes (18, 13 and 4 suppressors, respectively), we sequenced the genomic region inside the plasmids. Because most of the plasmids contained multiple genes, the genomic region of a single gene, including ORFs, 5′ and 3′ UTRs, and approximately 1.0 kb upstream and downstream sequences from the UTR, was amplified again via PCR and inserted into the pAL-SK vector (obtained from the National BioResource Project Yeast) at the BamHI site. The plasmids were then introduced into H1N1429, H1N1435 and H1N1436 cells to identify the genes responsible for rescuing growth.

Plasmid construction
All plasmids used in this study were constructed using the NEBuilder system (New England Biolabs, Ipswich, MA, USA; E2621L), according to the manufacturer's protocol. Restriction enzymes were purchased from TaKaRa Bio (Shiga, Japan) and New England Biolabs. For fluorescently tagged protein expression in mammalian cells, cDNA sequences for the protein of interest were amplified by PCR from a homemade cDNA pool generated by the following procedures. Total RNA was isolated from hTERT-RPE1 cells using ISOGEN (Nippongene, Tokyo, Japan; 311-02503), according to the manufacturer's protocol. The cDNA pool was generated from total RNA using the Superscript III First-Strand Synthesis System (Invitrogen, Waltham, MA, USA; 18080051) as a random hexamer primer for reverse transcription. PCR products were cloned into the pEF1α-EGFP-N1 vector, in which the cytomegalovirus promoter of the pEGFP-N1 vector (Clontech) was replaced with the EF1α promoter.

Spot assay
S. pombe cells were cultured overnight in EMMG medium at 30°C to attain the logarithmic growth phase. Five-fold serially diluted cells were spotted on EMMG plates (initially 4.0×10³ cells were spotted) and cultured at 30°C for 3–4 days.

Microscopic observation
S. pombe cells were observed using a DeltaVision Elite system (GE Healthcare, Chicago, IL, USA) equipped with a pco.edge 4.2 sCMOS (PCO, Kelheim, Germany) and a 60× PlanApo N OSC oil-immersion objective lens (NA=1.4; Olympus, Tokyo, Japan). The intracellular localization of GFP-S65T (designated as 'GFP' throughout this paper) and mCherry fusion proteins was observed in living cells. For live-cell imaging, cells were cultured overnight in EMMG medium at 30°C to attain the logarithmic growth phase before placing them onto a coverslip (No.1 S; Matsunami, Osaka, Japan). For FM4-64 staining, the cells were incubated with 8 µM FM4-64 in YES for 30 min, washed twice, and then incubated for 90 min in YES. The cells were attached to glass via soybean lectin (Sigma-Aldrich, St. Louis, MO, USA; L1395) and covered with EMMG medium. Optical section images were presented after deconvolution using the built-in SoftWoRx software (v7.0.0), using the default setting with a homemade optical transfer function, unless otherwise noted.

For mammalian cells, plasmids expressing hTLCD proteins and ER (KDEL–mCherry) or Golgi (1–82 amino acid residues of β-1,4-galactosyltransferase 1 tagged with mCherry) markers were co-transfected using Lipofectamine 2000 (Thermo Fisher Scientific, Waltham, MA, USA; 11668019), according to the manufacturer's protocol. After overnight incubation, the cells were observed under live conditions using the DeltaVision system, as described above.

Chromatic aberration for multi-color images was corrected using the Chromagnon software (v0.90) using bleed-through fluorescence or Tetraspeck microsphere fluorescent beads (Invitrogen; T7280) images as a reference (Matsuda et al., 2018). The brightness of the images was changed using the Fiji software (Schindelin et al., 2012) for better visualization without changing the gamma settings.

Western blotting

Cells cultured in the appropriate minimum medium, as described above, were harvested at the mid-log phase by centrifugation. Cells were lysed in 1.85 N NaOH for 15 min on ice. Proteins were precipitated by the addition of 27.5% trichloroacetic acid. After washing the precipitated proteins twice with ice-cold acetone, the proteins were resolved in a resolving buffer (50 mM Tris-HCl pH 8.0 and 1% SDS). Protein concentration was quantified using a bicinchoninic acid assay (Thermo Fisher Scientific; 23225), according to the manufacturer's protocol. Equal amounts of total protein were subjected to SDS-PAGE and transferred to a polyvinylidene difluoride membrane. Fluorescent proteins were probed with anti-GFP polyclonal (1:2000 dilution; Rockland, Philadelphia, PA, USA; 600-401215) and anti-RFP polyclonal (1:5000 dilution; MBL, Nagoya, Japan; PM005) antibodies. V5-tagged proteins were probed with an anti-V5 antibody (1:2000 dilution; Bio-Rad, CA, USA; MCA1360GA). β-actin was probed with an anti-β-actin monoclonal antibody (1:2000 dilution; Abcam, Cambridge, UK; ab8227) as a loading control. The bands were detected using chemiluminescence (ImmunoStar LD; FUJIFILM Wako Pure Chemical; 296-69901).

Lipid analysis using LC-MS/MS

Cells of the *lem2* shut-off strain were pre-cultured overnight in EMMG liquid medium at 30°C. The cells were transferred into EMMG liquid medium in the presence or absence of thiamine, cultured at 30°C for 12 h, and harvested via centrifugation. cells (1.0×10^7) were suspended in 100 μl of H_2O and mixed with 375 μl of chloroform/methanol/12 N formic acid (100:200:1, v/v/v). As an internal standard, 50 pmol of t18:0-d_9C16:0 [*N*-palmitoyl(d_9) D-ribo-phytosphingosine; Avanti Polar Lipids, Alabaster, AL, USA] was added. The cells were lysed using a Multi-Beads Shocker (Yasui Kikai, Japan) at 2700 rpm for 10 cycles of 60 s on/off. Lipids were extracted via successive addition and mixing of 125 μl of chloroform and 125 μl of H_2O. The phases were separated via centrifugation [20,000 *g*, at room temperature (approximately 26°C) for 3 min], and the organic (lower) phase was recovered, dried and dissolved in 1 ml of chloroform/methanol (1:2, v/v). Lipids were subjected to LC-MS/MS analysis, as described previously (Kinuagsa et al., 2019; Ohno et al., 2017). Ceramide species composed of C20 phytosphingosine (t20:0) and a non-hydroxy FA were detected via multiple reaction monitoring, selecting *m/z* of specific ceramide species [M+H]$^+$ at Q1 and *m/z* 328.3, which corresponded to the C20 phytosphingosine fragment ion at Q3. Ceramide levels were determined from three independent experiments. The values obtained from each experiment were plotted as the mean±s.d. calculated from three experiments. The significance of the measurements was assessed via Dunnett's test using the JMP software v13.0 (JMP, Cary, NC, USA).

Minichromosome loss assay

The minichromosome loss assay was performed as previously described (Tange et al., 2016). In this assay, a minichromosome Ch16 bearing the *ade6-216* allele was introduced into cells bearing the *ade6-210* allele. Cells carrying the minichromosome (*ade*$^+$) produced white colonies, whereas those lacking the minichromosome (*ade*$^-$) produced red colonies. Thus, a colony with a red–white half-sector indicates that the parental cell lost the minichromosome during the first cell division on the plate (Javerzat et al., 1996). Cells harboring minichromosome Ch16 were precultured in the EMMG liquid medium, plated on yeast extract (YE) plates, and incubated at 30°C for 3–4 days. For quantification, the number of colonies with a red sector in at least half of the colony was counted as half-sectored colonies. The rate of the minichromosome loss was calculated by dividing the number of half-sectored colonies by the total number of white and half-sectored colonies.

Quantification, statistics and reproducibility

To quantify the nuclear/cytoplasmic ratio of the GFP–GST–NLS signal, the nuclear and cytoplasmic regions in the original unprocessed image were manually marked as regions of interest (ROIs) using the Fiji software. After subtraction of the background noise measured outside the cells, the mean fluorescence intensities of the ROIs were measured. Fold enrichment (mean intensity ratio of nucleus/cytoplasm) was calculated and categorized into three groups (N/C>10, 10≥N/C≥ 3 and N/C<3). Significance was assessed via χ^2-test using GraphPad Prism 9.4.1 (San Diego, CA, USA).

To quantify the fluorescence intensity at the Golgi and NE in the *lem2* shut-off condition, we first projected z-stack images by sum projection and subtracted the background signal measured in regions outside the cells. The Golgi and NE were segmented by appropriate thresholding together with manual correction, and total fluorescence intensities at the Golgi and NE were measured using the default function in Fiji. Total fluorescence intensity in the cell was also quantified, and the percentages of fluorescence intensity at the Golgi and NE were calculated. Significance was assessed via an unpaired two-tailed Student's *t*-test using GraphPad Prism 9.5.0.

For phenotypic quantification, images were collected from at least three independent experiments. The numbers of Tlc4 foci and Golgi were counted in each experiment (the number of cells examined is mentioned in the figure legends), and the values were plotted as a Superplot (Lord et al., 2020). Significance was assessed via an unpaired two-tailed Student's *t*-test using GraphPad Prism 9.4.1.

Online supplementary material

Fig. S1 shows identified suppressors to rescue the growth defect in the *lem2Δbqt4Δ* double-deletion mutant. Fig. S2 shows an amino acid sequence alignment of the TLC domains. Fig. S3 shows that Tlc4 is localized to the NE/ER but not the vacuoles. Fig. S4 shows the predicted three-dimensional structure of Tlc4 mutants. Fig. S5 shows that hTLCD2, 3B and 5 are localized to the ER and Golgi. Fig. S6 shows the complementation assay using hTLCD. Fig. S7 shows that mutation in Lac1 corresponding to the R214 residue in Tlc4 alters the CerS activity. Fig. S8 shows a model of possible roles for Lem2, Bqt4 and Tlc4. Table S1 lists *S. pombe* strains used in this study.

Data availability
The data supporting the findings of this study are available within the paper and its supplementary information. Additional datasets are available from the corresponding authors upon reasonable request.

First Person
This article has an associated First Person interview with the first author of the paper.

References
Asakawa, H., Hirano, Y., Shindo, T., Haraguchi, T. and Hiraoka, Y. (2022). Fission yeast Ish1 and Les1 interact with each other in the lumen of the nuclear envelope. *Genes Cells* 27, 643-656. doi:10.1111/gtc.12981

Bähler, J., Wu, J. Q., Longtine, M. S., Shah, N. G., Mckenzie, A., Steever, A. B., Wach, A., Philippsen, P. and Pringle, J. R. (1998). Heterologous modules for

efficient and versatile PCR-based gene targeting in *Schizosaccharomyces pombe*. *Yeast* **14**, 943-951. doi:10.1002/(SICI)1097-0061(199807)14:10<943::AID-YEA292>3.0.CO;2-Y

Bahmanyar, S. and Schlieker, C. (2020). Lipid and protein dynamics that shape nuclear envelope identity. *Mol. Biol. Cell* **31**, 1315-1323. doi:10.1091/mbc.E18-10-0636

Banday, S., Farooq, Z., Rashid, R., Abdullah, E. and Altaf, M. (2016). Role of inner nuclear membrane protein complex Lem2-Nur1 in heterochromatic gene silencing. *J. Biol. Chem.* **291**, 20021-20029. doi:10.1074/jbc.M116.743211

Barrales, R. R., Forn, M., Georgescu, P. R., Sarkadi, Z. and Braun, S. (2016). Control of heterochromatin localization and silencing by the nuclear membrane protein Lem2. *Genes Dev.* **30**, 133-148. doi:10.1101/gad.271288.115

Cameron, J. R., Philippsen, P. and Davis, R. W. (1977). Analysis of chromosomal integration and deletions of yeast plasmids. *Nucleic Acids Res.* **4**, 1429-1448. doi:10.1093/nar/4.5.1429

Chikashige, Y., Yamane, M., Okamasa, K., Tsutsumi, C., Kojidani, T., Sato, M., Haraguchi, T. and Hiraoka, Y. (2009). Membrane proteins Bqt3 and –4 anchor telomeres to the nuclear envelope to ensure chromosomal bouquet formation. *J. Cell Biol.* **187**, 413-427. doi:10.1083/jcb.200902122

Denais, C. M., Gilbert, R. M., Isermann, P., Mcgregor, A. L., Te Lindert, M., Weigelin, B., Davidson, P. M., Friedl, P., Wolf, K. and Lammerding, J. (2016). Nuclear envelope rupture and repair during cancer cell migration. *Science* **352**, 353-358. doi:10.1126/science.aad7297

Dey, G., Culley, S., Curran, S., Schmidt, U., Henriques, R., Kukulski, W. and Baum, B. (2020). Closed mitosis requires local disassembly of the nuclear envelope. *Nature* **585**, 119-123. doi:10.1038/s41586-020-2648-3

Elagoz, A., Callejo, M., Armstrong, J. and Rokeach, L. A. (1999). Although calnexin is essential in *S. pombe*, its highly conserved central domain is dispensable for viability. *J. Cell Sci.* **112**, 4449-4460. doi:10.1242/jcs.112.23.4449

Flor-Parra, I., Sabido-Bozo, S., Ikeda, A., Hanaoka, K., Aguilera-Romero, A., Funato, K., Muñiz, M. and Lucena, R. (2021). The ceramide synthase subunit lac1 regulates cell growth and size in fission yeast. *Int. J. Mol. Sci.* **23**, 303. doi:10.3390/ijms23010303

Garton, S., Michaelson, L. V., Beaudoin, F., Beale, M. H. and Napier, J. A. (2003). The dihydroceramide desaturase is not essential for cell viability in Schizosaccharomyces pombe. *FEBS Lett.* **538**, 192-196. doi:10.1016/S0014-5793(03)00163-7

Gu, M., Lajoie, D., Chen, O. S., Von Appen, A., Ladinsky, M. S., Redd, M. J., Nikolova, L., Bjorkman, P. J., Sundquist, W. I., Ullman, K. S. et al. (2017). LEM2 recruits CHMP7 for ESCRT-mediated nuclear envelope closure in fission yeast and human cells. *Proc. Natl. Acad. Sci. USA* **114**, E2166-E2175. doi:10.1073/pnas.1616649114

Guillas, I., Kirchman, P. A., Chuard, R., Pfefferli, M., Jiang, J. C., Jazwinski, S. M. and Conzelmann, A. (2001). C26-CoA-dependent ceramide synthesis of *Saccharomyces cerevisiae* is operated by Lag1p and Lac1p. *EMBO J.* **20**, 2655-2665. doi:10.1093/emboj/20.11.2655

Güttinger, S., Laurell, E. and Kutay, U. (2009). Orchestrating nuclear envelope disassembly and reassembly during mitosis. *Nat. Rev. Mol. Cell Biol.* **10**, 178-191. doi:10.1038/nrm2641

Hanada, K., Kumagai, K., Yasuda, S., Miura, Y., Kawano, M., Fukasawa, M. and Nishijima, M. (2003). Molecular machinery for non-vesicular trafficking of ceramide. *Nature* **426**, 803-809. doi:10.1038/nature02188

Harris, M. A., Rutherford, K. M., Hayles, J., Lock, A., Bähler, J., Oliver, S. G., Mata, J. and Wood, V. (2022). Fission stories: using PomBase to understand *Schizosaccharomyces pombe* biology. *Genetics* **220**, iyab222. doi:10.1093/genetics/iyab222

Hirano, Y., Kinugasa, Y., Asakawa, H., Chikashige, Y., Obuse, C., Haraguchi, T. and Hiraoka, Y. (2018). Lem2 is retained at the nuclear envelope through its interaction with Bqt4 in fission yeast. *Genes Cells* **23**, 122-135. doi:10.1111/gtc.12557

Hirano, Y., Kinugasa, Y., Osakada, H., Shindo, T., Kubota, Y., Shibata, S., Haraguchi, T. and Hiraoka, Y. (2020). Lem2 and Lnp1 maintain the membrane boundary between the nuclear envelope and endoplasmic reticulum. *Commun. Biol.* **3**, 276. doi:10.1038/s42003-020-0999-9

Hu, C., Inoue, H., Sun, W., Takeshita, Y., Huang, Y., Xu, Y., Kanoh, J. and Chen, Y. (2019a). Structural insights into chromosome attachment to the nuclear envelope by an inner nuclear membrane protein Bqt4 in fission yeast. *Nucleic Acids Res.* **47**, 1573-1584. doi:10.1093/nar/gky1186

Hu, C., Inoue, H., Sun, W., Takeshita, Y., Huang, Y., Xu, Y., Kanoh, J. and Chen, Y. (2019b). The inner nuclear membrane protein Bqt4 in fission yeast contains a DNA-binding domain essential for telomere association with the nuclear envelope. *Structure* **27**, 335-343.e3. doi:10.1016/j.str.2018.10.010

Hull, C. M., Bader, O., Parker, J. E., Weig, M., Gross, U., Warrilow, A. G. S., Kelly, D. E. and Kelly, S. L. (2012). Two clinical isolates of candida glabrata exhibiting reduced sensitivity to amphotericin B both harbor mutations in *ERG2*. *Antimicrob. Agents Chemother.* **56**, 6417-6421. doi:10.1128/AAC.01145-12

Hwang, S., Williams, J. F., Kneissig, M., Lioudyno, M., Rivera, I., Helguera, P., Busciglio, J., Storchova, Z., King, M. C. and Torres, E. M. (2019). Suppressing aneuploidy-associated phenotypes improves the fitness of trisomy 21 cells. *Cell Rep.* **29**, 2473-2488.e5. doi:10.1016/j.celrep.2019.10.059

Ikeda, A., Schlarmann, P., Kurokawa, K., Nakano, A., Riezman, H. and Funato, K. (2020). Tricalbins are required for non-vesicular ceramide transport at ER-golgi contacts and modulate lipid droplet biogenesis. *iScience* **23**, 101603. doi:10.1016/j.isci.2020.101603

Imgrund, S., Hartmann, D., Farwanah, H., Eckhardt, M., Sandhoff, R., Degen, J., Gieselmann, V., Sandhoff, K. and Willecke, K. (2009). Adult ceramide synthase 2 (CERS2)-deficient mice exhibit myelin sheath defects, cerebellar degeneration, and hepatocarcinomas. *J. Biol. Chem.* **284**, 33549-33560. doi:10.1074/jbc.M109.031971

Ishii, M., Suda, Y., Kurokawa, K. and Nakano, A. (2016). COPI is essential for Golgi cisternal maturation and dynamics. *J. Cell Sci.* **129**, 3251-3261. doi:10.1242/jcs.193367

Javerzat, J. P., Cranston, G. and Allshire, R. C. (1996). Fission yeast genes which disrupt mitotic chromosome segregation when overexpressed. *Nucleic Acids Res.* **24**, 4676-4683. doi:10.1093/nar/24.23.4676

Kageyama-Yahara, N. and Riezman, H. (2006). Transmembrane topology of ceramide synthase in yeast. *Biochem. J.* **398**, 585-593. doi:10.1042/BJ20060697

Kihara, A. (2016). Synthesis and degradation pathways, functions, and pathology of ceramides and epidermal acylceramides. *Prog. Lipid Res.* **63**, 50-69. doi:10.1016/j.plipres.2016.04.001

Kinuagsa, Y., Hirano, Y., Sawai, M., Ohno, Y., Shindo, T., Asakawa, H., Chikashige, Y., Shibata, S., Kihara, A., Haraguchi, T. et al. (2019). The very-long-chain fatty acid elongase Elo2 rescues lethal defects associated with loss of the nuclear barrier function. *J. Cell Sci.* **132**, jcs229021. doi:10.1242/jcs.229021

Kume, K., Cantwell, H., Burrell, A. and Nurse, P. (2019). Nuclear membrane protein Lem2 regulates nuclear size through membrane flow. *Nat. Commun.* **10**, 1871. doi:10.1038/s41467-019-09623-x

Kurokawa, K., Okamoto, M. and Nakano, A. (2014). Contact of cis-Golgi with ER exit sites executes cargo capture and delivery from the ER. *Nat. Commun.* **5**, 3653. doi:10.1038/ncomms4653

Lajoie, D. and Ullman, K. S. (2017). Coordinated events of nuclear assembly. *Curr. Opin. Cell Biol.* **46**, 39-45. doi:10.1016/j.ceb.2016.12.008

Lee, I.-J., Stokasimov, E., Dempsey, N., Varberg, J. M., Jacob, E., Jaspersen, S. L. and Pellman, D. (2020). Factors promoting nuclear envelope assembly independent of the canonical ESCRT pathway. *J. Cell Biol.* **219**, e201998232. doi:10.1083/jcb.201908232

Levy, M. and Futerman, A. H. (2010). Mammalian ceramide synthases. *IUBMB Life* **62**, 237-246. doi:10.1002/iub.314

Limar, S., Körner, C., Martínez-Montañés, F., Stancheva, V. G., Wolf, V. N., Walter, S., Miller, E. A., Ejsing, C. S., Galassi, V. V. and Fröhlich, F. (2023). Yeast Svf1 binds ceramides and contributes to sphingolipid metabolism at the ER cis-Golgi interface. *J. Cell Biol.* **222**, e202109162. doi:10.1083/jcb.202109162

Liu, L.-K., Choudhary, V., Toulmay, A. and Prinz, W. A. (2017). An inducible ER–Golgi tether facilitates ceramide transport to alleviate lipotoxicity. *J. Cell Biol.* **216**, 131-147. doi:10.1083/jcb.201606059

Lord, S. J., Velle, K. B., Mullins, R. D. and Fritz-Laylin, L. K. (2020). SuperPlots: communicating reproducibility and variability in cell biology. *J. Cell Biol.* **219**, e202001064. doi:10.1083/jcb.202001064

Mallela, S. K., Almeida, R., Ejsing, C. S. and Conzelmann, A. (2016). Functions of ceramide synthase paralogs YPR114w and YJR116w of *Saccharomyces cerevisiae*. *PLoS One* **11**, e0145831. doi:10.1371/journal.pone.0145831

Martín Caballero, L., Capella, M., Barrales, R. R., Dobrev, N., Van Emden, T., Hirano, Y., Suma Sreechakram, V. N., Fischer-Burkart, S., Kinugasa, Y., Nevers, A. et al. (2022). The inner nuclear membrane protein Lem2 coordinates RNA degradation at the nuclear periphery. *Nat. Struct. Mol. Biol.* **29**, 910-921. doi:10.1038/s41594-022-00831-6

Matsuda, A., Schermelleh, L., Hirano, Y., Haraguchi, T. and Hiraoka, Y. (2018). Accurate and fiducial-marker-free correction for three-dimensional chromatic shift in biological fluorescence microscopy. *Sci. Rep.* **8**, 7583. doi:10.1038/s41598-018-25922-7

Mirdita, M., Schütze, K., Moriwaki, Y., Heo, L., Ovchinnikov, S. and Steinegger, M. (2022). ColabFold: making protein folding accessible to all. *Nat. Methods* **19**, 679-682. doi:10.1038/s41592-022-01488-1

Mizutani, Y., Mitsutake, S., Tsuji, K., Kihara, A. and Igarashi, Y. (2009). Ceramide biosynthesis in keratinocyte and its role in skin function. *Biochimie* **91**, 784-790. doi:10.1016/j.biochi.2009.04.001

Moreno, S., Klar, A. and Nurse, P. (1991). Molecular genetic analysis of fission yeast *Schizosaccharomyces pombe*. *Methods Enzymol.* **194**, 795-823. doi:10.1016/0076-6879(91)94059-L

Núñez, A., Dulude, D., Jbel, M. and Rokeach, L. A. (2015). Calnexin is essential for survival under nitrogen starvation and stationary phase in *Schizosaccharomyces pombe*. *PLoS One* **10**, e0121059. doi:10.1371/journal.pone.0121059

Ohno, Y., Kamiyama, N., Nakamichi, S. and Kihara, A. (2017). PNPLA1 is a transacylase essential for the generation of the skin barrier lipid ω-O-acylceramide. *Nat. Commun.* **8**, 14610. doi:10.1038/ncomms14610

Olmos, Y., Hodgson, L., Mantell, J., Verkade, P. and Carlton, J. G. (2015). ESCRT-III controls nuclear envelope reformation. *Nature* **522**, 236-239. doi:10.1038/nature14503

Parlati, F., Dignard, D., Bergeron, J. J. and Thomas, D. Y. (1995). The calnexin homologue *cnx1+* in *Schizosaccharomyces pombe*, is an essential gene which can be complemented by its soluble ER domain. *EMBO J.* **14**, 3064-3072. doi:10.1002/j.1460-2075.1995.tb07309.x

Penfield, L., Shankar, R., Szentgyörgyi, E., Laffitte, A., Mauro, M. S., Audhya, A., Müller-Reichert, T. and Bahmanyar, S. (2020). Regulated lipid synthesis and LEM2/CHMP7 jointly control nuclear envelope closure. *J. Cell Biol.* **219**, e201908179. doi:10.1083/jcb.201908179

Petkevicius, K., Palmgren, H., Glover, M. S., Ahnmark, A., Andréasson, A.-C., Madeyski-Bengtson, K., Kawana, H., Allman, E. L., Kaper, D., Uhrbom, M. et al. (2022). TLCD1 and TLCD2 regulate cellular phosphatidylethanolamine composition and promote the progression of non-alcoholic steatohepatitis. *Nat. Commun.* **13**, 6020. doi:10.1038/s41467-022-33735-6

Pieper, G. H., Sprenger, S., Teis, D. and Oliferenko, S. (2020). ESCRT-III/Vps4 controls heterochromatin-nuclear envelope attachments. *Dev. Cell* **53**, 27-41.e6. doi:10.1016/j.devcel.2020.01.028

Raab, M., Gentili, M., De Belly, H., Thiam, H. R., Vargas, P., Jimenez, A. J., Lautenschlaeger, F., Voituriez, R., Lennon-Duménil, A. M., Manel, N. et al. (2016). ESCRT III repairs nuclear envelope ruptures during cell migration to limit DNA damage and cell death. *Science* **352**, 359-362. doi:10.1126/science.aad7611

Schindelin, J., Arganda-Carreras, I., Frise, E., Kaynig, V., Longair, M., Pietzsch, T., Preibisch, S., Rueden, C., Saalfeld, S., Schmid, B. et al. (2012). Fiji: an open-source platform for biological-image analysis. *Nat. Methods* **9**, 676-682. doi:10.1038/nmeth.2019

Schlarmann, P., Ikeda, A. and Funato, K. (2021). Membrane contact sites in yeast: control hubs of sphingolipid homeostasis. *Membranes* **11**, 971. doi:10.3390/membranes11120971

Schorling, S., Vallée, B., Barz, W. P., Riezman, H. and Oesterhelt, D. (2001). Lag1p and Lac1p Are essential for the Acyl-CoA–dependent ceramide synthase reaction in *Saccharomyces cerevisae*. *Mol. Biol. Cell* **12**, 3417-3427. doi:10.1091/mbc.12.11.3417

Spassieva, S., Seo, J.-G., Jiang, J. C., Bielawski, J., Alvarez-Vasquez, F., Jazwinski, S. M., Hannun, Y. A. and Obeid, L. M. (2006). Necessary role for the Lag1p motif in (Dihydro)ceramide synthase activity. *J. Biol. Chem.* **281**, 33931-33938. doi:10.1074/jbc.M608092200

Tange, Y., Chikashige, Y., Takahata, S., Kawakami, K., Higashi, M., Mori, C., Kojidani, T., Hirano, Y., Asakawa, H., Murakami, Y. et al. (2016). Inner nuclear membrane protein Lem2 augments heterochromatin formation in response to nutritional conditions. *Genes Cells* **21**, 812-832. doi:10.1111/gtc.12385

Thaller, D. J., Tong, D., Marklew, C. J., Ader, N. R., Mannino, P. J., Borah, S., King, M. C., Ciani, B. and Lusk, C. P. (2021). Direct binding of ESCRT protein Chm7 to phosphatidic acid–rich membranes at nuclear envelope herniations. *J. Cell Biol.* **220**, e202004222. doi:10.1083/jcb.202004222

Ungricht, R. and Kutay, U. (2017). Mechanisms and functions of nuclear envelope remodelling. *Nat. Rev. Mol. Cell Biol.* **18**, 229-245. doi:10.1038/nrm.2016.153

Vietri, M., Schink, K. O., Campsteijn, C., Wegner, C. S., Schultz, S. W., Christ, L., Thoresen, S. B., Brech, A., Raiborg, C. and Stenmark, H. (2015). Spastin and ESCRT-III coordinate mitotic spindle disassembly and nuclear envelope sealing. *Nature* **522**, 231-235. doi:10.1038/nature14408

Von Appen, A., Lajoie, D., Johnson, I. E., Trnka, M. J., Pick, S. M., Burlingame, A. L., Ullman, K. S. and Frost, A. (2020). LEM2 phase separation promotes ESCRT-mediated nuclear envelope reformation. *Nature* **582**, 115-118. doi:10.1038/s41586-020-2232-x

Wach, A. (1996). PCR-synthesis of marker cassettes with long flanking homology regions for gene disruptions in *S. cerevisiae*. *Yeast* **12**, 259-265. doi:10.1002/(SICI)1097-0061(19960315)12:3<259::AID-YEA901>3.0.CO;2-C

Webster, B. M. and Lusk, C. P. (2016). Border safety: quality control at the nuclear envelope. *Trend Cell Biol.* **26**, 29-39. doi:10.1016/j.tcb.2015.08.002

Webster, B. M., Thaller, D. J., Jäger, J., Ochmann, S. E., Borah, S. and Lusk, C. P. (2016). Chm7 and Heh1 collaborate to link nuclear pore complex quality control with nuclear envelope sealing. *EMBO J.* **35**, 2447-2467. doi:10.15252/embj.201694574

Williams, R. L. and Urbé, S. (2007). The emerging shape of the ESCRT machinery. *Nat. Rev. Mol. Cell Biol.* **8**, 355-368. doi:10.1038/nrm2162

Winter, E. and Ponting, C. P. (2002). TRAM, LAG1 and CLN8: members of a novel family of lipid-sensing domains? *Trends Biochem. Sci.* **27**, 381-383. doi:10.1016/S0968-0004(02)02154-0